Biomaterials 239 (2020) 119846

Contents lists available at ScienceDirect

Biomaterials

journal homepage: www.elsevier.com/locate/biomaterials

Comparative effects of N-cadherin protein and peptide fragments on mesenchymal stem cell mechanotransduction and paracrine function

Ellen C. Qin[a], Syeda T. Ahmed[b], Poonam Sehgal[c], Vinh H. Vu[c], Hyunjoon Kong[b,d,e,f,*], Deborah E. Leckband[b,c,d,e,f,g,**]

[a] Department of Materials Science and Engineering, University of Illinois, Urbana Champaign, USA
[b] Department of Chemical and Biomolecular Engineering, University of Illinois, Urbana Champaign, USA
[c] Department of Biochemistry, University of Illinois, Urbana Champaign, USA
[d] Department of Bioengineering, University of Illinois, Urbana Champaign, USA
[e] Carl R. Woese Institute for Genomic Biology, University of Illinois, Urbana Champaign, USA
[f] Beckman Institute, University of Illinois, Urbana Champaign, IL, USA
[g] Department of Chemistry, University of Illinois, Urbana Champaign, IL, USA

ARTICLE INFO

Keywords:
N-Cadherin
HAVDI Peptide
Mechanotransduction
Paracrine function
Hydrogel
Mesenchymal stem cell

ABSTRACT

The recent interest in exploiting cadherin-derived fragments to mimic intercellular adhesion in engineered hybrid biomaterials raises questions about which cadherin constructs effectively mimic cadherin interactions. This study compared the biophysical properties of and signaling initiated by three different, immobilized N-cadherin-derived fragments, in order to identify a minimal construct that mimics intercellular adhesion in biomaterials. Specifically, we compared: i) the full N-cadherin extracellular region with all five ectodomains (EC1-5), ii) the first two ectodomains (EC1-2) of N-cadherin, and iii) a peptide containing the histidine-alanine-valine-aspartic acid-valine (HAVDI) sequence in the first extracellular domain. Comparisons of the binding kinetics and affinities between each of these ligands and N-cadherin expressed on mesenchymal stem cells (MSCs) revealed quantitative differences. Nevertheless, MSCs exhibited similar, rigidity-dependent spreading and traction forces when cultured on gels displaying any of these N-cadherin ligands. There were, however, differences in cell signaling and secretory activities. MSCs cultured on the full N-cadherin extracellular domain (EC1-5) exhibited stiffness-dependent changes in nuclear YAP/TAZ localization and significantly higher secretion of vascular endothelial growth factor and insulin growth factor 1, compared to cells cultured on hydrogels displaying either EC1-2 or the HAVDI peptide. The increased paracrine secretion also enhanced myogenic differentiation. These findings reveal functional differences between N-cadherin derived ligands important for the design of biomaterials that mimic intercellular adhesion.

1. Introduction

Cadherins are calcium-dependent cell-cell adhesion proteins that are essential for tissue morphogenesis [1–6], cell recognition and sorting in tissue formation [6–8], and coordinated cell movements [9]. Cadherin adhesion activates signal cascades that regulate cytoskeletal organization [10], cell migration [9,11], differentiation [12–14], and proliferation [15–17]. Cadherins are force transducers that activate cytoskeletal remodeling and signaling in response to changes in intercellular tension [18].

Due to the diversity of cadherin-dependent biological processes, there is increased interest in the use of cadherin-derived ligands as

Abbreviations: MSC, Mesenchymal stem cells; N-cad, N-cadherin; N-cad EC1-5 or N-cad Fc, Fc-tagged N-cadherin with ectodomains 1 to 5; N-cad EC1-2, Biotinylated N-cadherin with ectodomains 1 and 2; HAVDI, Histidine-Alanine-Valine-Aspartic Acid-Isoleucine peptide; Scramb, Scrambled peptide; PDL, poly-*d*-lysine; YAP/TAZ, *Yorkie*-homologues Yes-Associated Protein with Transcriptional Co-Activator with PDZ-binding motif; RBC, Red blood cell; VEGF, Vascular endothelial growth factor; IGF-1, Insulin-like growth factor 1; MSC-CDM, Mesenchymal stem cell conditioned differentiation medium

* Corresponding author. Department of Chemical and Biomolecular Engineering, University of Illinois, 600 South Mathews Avenue, 108 RAL, Urbana, IL, 61801, USA.

** Corresponding author. Departments of Chemical and Biomolecular Engineering and Chemistry, University of Illinois, 600 South Mathews Avenue, 127 RAL, Box C-3, Urbana, IL, 61801, USA.

E-mail addresses: hjkong06@illinois.edu (H. Kong), leckband@illinois.edu (D.E. Leckband).

https://doi.org/10.1016/j.biomaterials.2020.119846
Received 20 August 2019; Received in revised form 4 February 2020; Accepted 4 February 2020
Available online 10 February 2020
0142-9612/

potential biochemical cues in engineered hybrid biomaterials, analogous to the use of integrin ligands [19]. Over 20 different classical cadherin subtypes exist, and they are named according to the tissue from which they were first isolated [2,20]. The different cadherin subtypes can activate similar signaling pathways; however, subtype-dependent differences raise the possibility of exploiting cadherins to instruct tissue-specific functions. Among these, neural (N-) cadherin and epithelial (E−) cadherins are two classical cadherin subtypes that are expressed on mesenchymal stem cells (MSCs). N-cadherin, specifically, is involved in the mechanotransduction [21], paracrine function [22–24], and differentiation [21,25,26] of MSCs.

To recapitulate N-cadherin interactions *in vitro*, biomaterials have been modified with either the Fc-tagged N-cadherin extracellular domain (N-cad-Fc) [27–30] or peptides containing the highly conserved histidine-alanine-valine (HAV) sequence in the first extracellular domain (EC1) of all classical cadherins [21,24–26]. The adhesion of N-cadherin expressing cells to immobilized N-cad-Fc activates typical N-cadherin signaling and cytoskeletal remodeling [10,31–33]. Other studies showed that incorporating the HAV peptide sequence into a methacrylated hyaluronic acid backbone influences the fate commitment of MSCs and alters the mechano-sensitivity of the stem cell to the stiffening extracellular microenvironment [21,34]. Additional studies have suggested that the HAVDI peptide suppresses the canonical Wnt/β-catenin signaling, which enhances the chondrogenesis of MSCs [35]. These results suggest that both immobilized N-cad-Fc and HAV-containing peptides support N-cadherin mediated cell adhesion and potentiate N-cadherin-specific functions. However, the minimal fragment that mimics N-cadherin dependent adhesive functions is unclear, especially when considering the established mechanism of cadherin binding [20].

Classical cadherins are composed of an extracellular domain, a single transmembrane domain, and a cytoplasmic domain [20]. The extracellular domain, which contains the adhesive interface comprises five tandem extracellular (EC) domain repeats (EC1-5) [2,36]. Structural and biochemical data show that cadherins on opposing cells bind through their N-terminal EC1 domains (Fig. 1a). The established mechanism involves the formation of a 'strand swapped' dimer in which the tryptophan at position 2 (W2) from one protein docks in a hydrophobic pocket of the EC1 domain on the opposing cadherin (Fig. 1a) [20,36–38]. The W2 amino acid is conserved across all classical cadherins, as is an HAV sequence within the same domain (Fig. 1a) [20,39].

The complete adhesive interface between opposing cadherins requires two tryptophans and two binding pockets (Fig. 1a). Differences in reported contacts between the HAV side chains and tryptophan at position 2 (W2) in crystal structures raise questions about the role of this conserved sequence in cadherin adhesion [38,40]. In crystal structures, the HAV sequence forms part of the hydrophobic W2 binding pocket. However, alanine makes little direct contact with the docked tryptophan because it is partially obscured and oriented into the protein core away from the binding pocket; only histidine and valine form lattice contacts with W2 and account for less than 5% of the entire binding interface [38,40]. Intriguingly, an early study showed that a synthetic peptide containing a single HAV sequence inhibited both compaction of mouse embryos and neurite outgrowth on astrocytes [39]. Furthermore, cyclic peptides containing HAV sequences in tandem have also been shown to promote the survival of neurons by linking two neurites together [41]. The addition of aspartic acid (D) and isoleucine (I) to form a peptide motif HAVDI improved the specificity of the sequence for N-cadherin [42]. In the context of the established binding mechanism (Fig. 1a), the underlying mechanism of these peptide interactions is unknown.

Two additional features that involve regions outside of the EC1 domain contribute to cadherin-mediated adhesion [18]. Cadherins form a catch bond that forms at the junctions between EC1 and EC2 domains [43,44]. This 'X-dimer' appears to be a kinetic intermediate in the strand swapping pathway [45], such that the X-dimer and both EC1 and EC2 might also be required for adhesion. HAV containing peptides may bind W2, but they cannot form the intermediate. Additional studies reported that ectodomain fragments containing the first three extracellular domains EC1-3 exhibit a distinct kinetic binding signature [46–49], and they facilitate lateral cadherin clustering at intercellular adhesions [45,50].

These different features of cadherin binding and clustering raise questions regarding the minimal fragment required to mimic N-cadherin dependent adhesion and adhesion-dependent signaling in engineered scaffolds. Here, we compared the biophysical and signaling properties of three different N-cadherin ligands that contain structural regions that support different features of the cadherin binding mechanism: 1) an Fc-tagged N-cadherin recombinant protein with all five extracellular domains (N-cad EC1-5); 2) a biotinylated N-cadherin fragment containing EC1 and EC2 (N-cad EC1-2); and 3) a peptide containing the Histidine-Alanine-Valine-Aspartate-Isoleucine (HAVDI) sequence, which has greater affinity for N-cadherin than HAV alone. All three of the N-cadherin ligands contain potential cadherin binding interfaces, but only N-cad EC1-2 and N-cad EC1-5 contain the W2 residue, the W2 binding pocket, and the X-dimer interface. Only N-cad EC1-5 contains the interface postulated to support lateral cadherin clustering [49,51]. We quantified similarities and differences of binding affinities between these ligands and N-cadherin expressed on MSCs, as well as cell spreading, traction generation, and signaling in cells on substrates displaying the different proteins or peptides. The paracrine secretion of

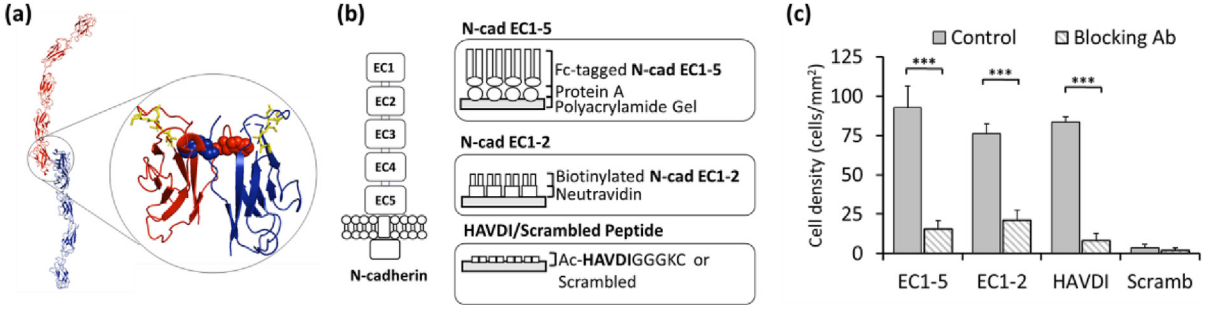

Fig. 1. Surface display of immobilized N-cadherin ligands and cell attachment efficiencies. (a) Cadherin binding mechanism. The red and blue ribbons indicate the extracellular domains of two different N-cadherin molecules from opposing cells. A magnified view of the EC1 domain is shown on the right. The HAVDI sequence is shown in yellow and the W2 residues participating in strand dimer exchange are shown as red vdW spheres. The protein files are from Protein Data Bank (PDB) accession 1NCH [38]. (b) Schematic showing the reaction scheme for immobilizing N-cadherin ligands on the hydrogels. A schematic of the full cadherin structure with the numbered EC domains is on the left. The panels indicate the different immobilization strategies used. (c) Quantified density of MSCs adhered on 10 kPa hydrogels with or without treatment with N-cadherin blocking (control) antibody. (n = 3 hydrogels per group; ***: $p < 0.001$; two-way ANOVA with Tukey-HSD post-hoc; mean ± s. e.m.). (For interpretation of the references to colour in this figure legend, the reader is referred to the Web version of this article.)

MSCs cultured on these N-cadherin ligands, as well as the effects of secreted paracrine factors on myogenic differentiation were also studied.

2. Materials and Methods

2.1. Production of Fc-tagged N-cadherin EC1-5

The soluble, recombinant N-cadherin extracellular region containing all five ectodomains with a C-terminal IgG Fc tag (N-cad EC1-5) was stably expressed in human embryonic kidney cells (HEK293, American Type Culture Collection), as previously described [31,46]. Cells were cultured in Dulbecco's Modified Eagle Medium (DMEM) supplemented with 10% (v/v) fetal bovine serum (FBS), 1% (v/v) Penicillin-Streptomycin (P/S) and 0.4 mg/mL G418 (Sigma Aldrich) as a selection agent. N-cad EC1-5 was purified from filtered cell culture supernatant, using a protein-A affinity column (Bio-Rad) followed by gel filtration chromatography (HiPrep 16/60 Sephacryl S-200 HR, Sigma-Aldrich) with an AKTA Pure protein purification system. Protein purity was assessed using sodium dodecyl sulfate polyacrylamide gel electrophoresis (SDS-PAGE). The Fc-tagged ectodomain has been shown to have the same affinity as cell surface cadherin [52].

2.2. Biotinylated N-cadherin EC1-2 design, expression, and purification

Escherichia coli BL21 (DE3) cells were co-transfected with two plasmids encoding the BirA ligase and a His_6-tagged N-cadherin EC1-2 fragment. The plasmid encoding BirA ligase (a gift from Prof. John E. Cronan, University of Illinois at Urbana Champaign) carries the BirA gene under the control of the araBAD promoter [53]. The N-cad EC1-2 plasmid was designed with an N-terminal Small Ubiquitin-like Modifiers (SUMO) Protease SUMO-tag, the first two ectodomains of N-cadherin (EC1-2), followed by a flexible Gly-Gly-Gly linker and Avi-tag. The sequence was cloned into a pRSET-A vector backbone with an N-terminal 6XHis tag (Suppl. Fig. S1). The SUMO-tag was PCR amplified from pRSF-KpDcr1 (Addgene) with BamH1 and Kpn1 restriction sites at the N- terminal and C-terminal sites, respectively. The N-cad EC1-2 cDNA was PCR amplified from a plasmid encoding the full-length human N-cadherin sequence, with Kpn1 and Nhe1 restriction sites at the N- and C-termini, respectively. Finally, an Avi-tag with a stop sequence was inserted between the Nhe1 and EcoR1 restriction sites. The entire sequence was cloned into the BamH1 and EcoR1 sites of the pRSET-A vector.

Escherichia coli BL21 (DE3) cells co-expressing His_6-tagged N-cad EC1-2 and the BirA ligase were grown overnight at 37 °C in Lennox LB medium supplemented with 5 mg/L of L-(+)-arabinose (Sigma Aldrich), 0.01% (w/v) biotin (Sigma Aldrich), 0.1 mg/mL ampicillin and 25 mg/mL chloramphenicol. The bacterial culture was diluted in fresh LB medium, at a ratio of 1:100 with the above supplements. When the optical density (OD) of the bacterial culture reached 0.4–0.6, isopropyl β-D-1-thiogalactopyranoside (IPTG) was added to the culture to a final concentration of 0.5 mM to induce the production of N-cad EC1-2. After 4 h, the bacterial culture was pelleted by centrifugation at 8,000 rpm for 10 min using a Sorvall RC-5C Plus centrifuge equipped with a GS3 rotor, and frozen at −20 °C. The frozen pellet was thawed and resuspended on ice in lysis buffer composed of Bugbuster® protein extraction reagent (3 mL/g wet weight of pellet; Millipore) supplemented with 1 mg/mL lysozyme (Sigma Aldrich) and 1x complete EDTA-free protease inhibitor cocktail (Roche, Mannheim, Germany). After 15 min, the culture was kept on ice and probe-sonicated for four cycles with 15 s bursts and 30 s rest intervals. The cell lysate was clarified by centrifugation at 15,000 rpm for 30 min using a Sorvall RC-5C Plus centrifuge and a SS34 rotor. The clarified supernatant was loaded onto an Ni-NTA agarose column (Qiagen) that was previously equilibrated with binding buffer (20 mM Tris - pH 7.4, 10 mM NaCl, 2 mM $CaCl_2$). The column was then rinsed with wash buffer (20 mM Tris - pH 7.4, 500 mM NaCl, 2 mM $CaCl_2$, and 20 mM imidazole) to remove unbound protein. The His_6-N-cad EC1-2 was eluted from the column with elution buffer (20 mM Tris - pH 7.4, 50 mM NaCl, 2 mM $CaCl_2$, and 250 mM imidazole). The eluted His_6-N-cad EC1-2 was concentrated and the buffer was exchanged with phosphate buffered saline containing 2 mM $CaCl_2$ (cPBS), by using a 10 kDa MWCO centrifugation filter (Millipore). The N-terminal His_6-tag was cleaved from the soluble N-cad EC1-2 protein using Small Ubiquitin-like Modifiers (SUMO) Protease (McLab). The reaction was performed in 1X SUMO Protease buffer (500 mM Tris-HCl, pH 8.0, 2% Igepal, 10 mM DTT) with 1 unit enzyme for every 2 μg of protein, at 4 °C for 2 h. The mixture was transferred to a Ni-NTA column (Qiagen), which separated the cleaved His6X-tag from the final biotinylated N-cad EC1-2. The purity of the eluted N-cad EC1-2 was determined by sodium dodecyl sulfate–polyacrylamide gel electrophoresis (SDS-PAGE), and the concentration was measured using a bicinchoninic acid (BCA) assay kit (Thermo Scientific).

2.3. HAVDI peptide

The N-cadherin-mimetic peptide (Ac-HAVDIGGGKC-OH) and scrambled peptide control (Ac-AGVGDGGGKC-OH) were purchased from Mimotopes (Minneapolis, US). The peptide sequence, with the exception of the additional lysine group, is the same as was used in prior studies to study cell behavior [21,24,34]. In both cases, the conjugation to the hydrogel was performed on the 10th amino acid from the N-terminus. A cysteine reactive Cy5-maleimide dye (GE Healthcare) was used to fluorescently label the cysteines on the peptides. For adhesion and traction measurements, peptides were directly coupled to polyacrylamide gels, but for kinetics measurements, the peptides were biotinylated and immobilized on Neutravidin (Sigma Aldrich). For the dye labeling reaction, peptides were dissolved in PBS to 2 mg/mL and reacted with the dye at a 1:2 peptide to dye molar ratio for 2 h at room temperature. For micropipette measurements, the peptide was biotinylated and immobilized on neutravidin bound to red blood cells. NHS-LC-biotin (Thermo Scientific) was used to biotinylate the peptides through the lysine group. The 22 Å spacer arm of this crosslinker projects the peptide well outside of the 10 Å deep neutravidin binding site. The peptide would be accessible to cell surface cadherins, whose binding sites at the tip of the N-terminal EC1 domain are ~250 Å from the membrane [36]. The peptides were dissolved in PBS at a concentration of 2 mg/mL, and reacted with NHS-LC-biotin at a 1:2 peptide:biotin molar ratio for 30 min at room temperature. The unconjugated fluorescent dye or unreacted NHS-LC-biotin were removed from the peptide with high-performance liquid chromatography (PerkinElmer Flexar), and the final products were analyzed by low-resolution electrospray ionization mass spectrometry (Waters Quattro II).

2.4. Preparation of protein and peptide-conjugated polyacrylamide hydrogels

Polyacrylamide hydrogels were prepared by free radical polymerization of the acrylamide monomer with the bis-acrylamide crosslinker, as previously described [54]. Glass bottomed dishes with 14 mm glass microwells were plasma treated to render the surface hydrophilic. Then, the glass was treated with 3-aminopropyl-triethoxysilane (APTES; Sigma-Aldrich) for 6 min and rinsed with deionized (DI) water. The glass was further treated with 0.5% glutaraldehyde (Sigma Aldrich) for 20 min, rinsed with DI water, and air-dried. Pre-gel solutions containing acrylamide (Sigma Aldrich) and bis-acrylamide (Sigma Aldrich) were prepared. The elastic modulus of the gel was varied, by controlling the concentration of acrylamide and bis-acrylamide. Hydrogels with an elastic modulus of 10 kPa were prepared with 5% (w/w) acrylamide and 0.3% (w/w) bis-acrylamide in water. Gels with an elastic modulus of 36 kPa were prepared with 8% (w/w) acrylamide and 0.48% (w/w) bis-acrylamide in water. Polymerization was initiated with the addition

of 5 μL 10% ammonium persulfate (APS; Sigma Aldrich) and 0.5 μL N,N,N′,N′-tetramethylethylenediamine (TEMED; Sigma-Aldrich) to 1 mL of the pre-gel solution. For traction force microscopy, 0.2 μm rhodamine beads (1:500; Invitrogen) were added to the pre-gel solution. After the addition of APS and TEMED, 20 μL of the mixture was placed at the center of the glass bottom dish and covered with a 12-mm glass coverslip. The dishes were immediately inverted during polymerization to allow the beads to settle by gravity near the surface. After 20 min, the gels were stored in DI water overnight to remove unreacted chemicals. Before use, the coverslip was removed from the gels, and the gels were sterilized by UV.

2.5. Protein and peptide immobilization on polyacrylamide hydrogels

The peptides were directly conjugated to the hydrogels, but the biotinylated N-cad EC1-2 and Fc-tagged N-cad EC1-5 proteins were bound and oriented on immobilized Neutravidin (Sigma Aldrich) and Protein A (Sigma Aldrich), respectively. To activate the hydrogels for protein and peptide immobilization, a stock solution of sulfosuccinimidyl 6-(40-azido-20-nitrophenylamino)hexanoate (sulfo-SANPAH, 25 mg/mL in dimethyl sulfoxide; Thermo Scientific) was diluted to 1 mg/mL in water, added to the hydrogel, and exposed to UV light (wavelength of 320 nm) for 8 min, before rinsing the gels with PBS. The HAVDI or scrambled peptide was immobilized directly by incubation of a 6 μg/mL HAVDI or scrambled peptide solution with the activated gel for 2 h at room temperature. To immobilize N-cad EC1-5, the activated gels were first incubated with 0.2 mg/mL protein A for 1 h at room temperature, rinsed with cPBS, and then incubated with 0.1 mg/mL Fc-tagged N-cad EC1-5 for 1 h at room temperature. Hydrogels modified with biotinylated N-cad EC1-2 were first incubated with 0.2 mg/mL Neutravidin (Sigma Aldrich) for 1 h at room temperature, rinsed with PBS, and then incubated with 0.06 mg/mL of biotinylated N-cad EC1-2 for 1 h at room temperature. For MSC differentiation studies, the proteins used in the first modification (with protein A, Neutravidin, or peptide) was also mixed with 10 μg/mL poly-D-lysine hydrobromide (PDL, Mw ~ 30,000–70,000; Sigma-Aldrich, Catalog #: P7280). For controls, hydrogels were modified with either 0.1 mg/mL type I collagen (Advanced BioMatrix) or 10 μg/mL of PDL, by incubation with the sulfo-SANPAH-activated hydrogels for 1 h at room temperature.

All hydrogels were prepared the day before cell culture experiments. After the protein incubations, the substrates were extensively washed and stored at 4 °C in cPBS before use. About 20 min before cell experiments, cPBS was replaced with DMEM at 37 °C.

2.6. Quantification of immobilized protein and peptide surface densities

The surface densities of N-cadherin ligands immobilized on the substrates were determined by material balance, using an ELISA assay. For N-cad EC1-5 and N-cad EC1-2, the protein solutions after incubation with the hydrogel in addition to two, subsequent washes were collected and added to a 96-well polystyrene plate. After incubation for 1 h at 37 °C, the wells were rinsed with cPBS, and then incubated with 2% bovine serum albumin (BSA) in cPBS for 1 h at 37 °C. Then, the wells containing N-cadherin fragments were incubated overnight at 4 °C with a rabbit, anti-N-cadherin polyclonal antibody that specifically binds to the EC1-2 domain (1:600 in cPBS with 2% BSA; ProteinTech, Catalog #: 13769-1-AP). The unbound antibody was then removed by rinsing with cPBS, and horseradish peroxidase (HRP)-conjugated anti-rabbit IgG (1:10,000 in cPBS with 2% BSA; Sigma Aldrich) was added to each well and incubated at room temperature for 1 h. A 3,3′,5,5′-tetramethylbenzidine (TMB) ELISA substrate kit (Thermo Fisher) was used as a chromogenic substrate for HRP. After incubation for 20 min with the TMB and peroxide solution, the absorbance of each well was measured at 370 nm with a microplate reader (Tecan Infinite 200 PRO). To relate the readouts to the amounts of protein in the initial wash solutions, a calibration curve was generated with known concentrations of the N-cadherin protein. The amount of protein bound to the hydrogels was then determined from the difference between the amount of protein added and the amount recovered in the wash solutions.

To determine the densities of peptides on the gels, fluorescently tagged peptides were bound to the surface of the hydrogels. The solutions containing unbound peptides were collected from the hydrogel substrates and added to a 96-well polystyrene plate. The absorbance of each well was measured at 649 nm with a microplate reader (Tecan Infinite 200 PRO), and the density of peptides was calculated using the Beer-Lambert law. Further details on the determination of the surface densities of immobilized protein or peptide is included in the Supplementary Material (Suppl. Fig. S2 and Table S1).

2.7. Cell culture

Clonally derived mouse bone marrow stromal mesenchymal stem cells (MSCs, D1 cells; ATCC, CRL-12424) were maintained at sub-confluence in standard MSC growth medium containing DMEM Dulbecco's Modification of Eagle's (DMEM) medium with 4.5 g/L glucose, L-gluatmine, and sodium pyruvate (Corning, Catalog #: 10-013-CV) supplemented with 10 v/v% FBS and 1 v/v% P/S. Prior to studies for cell adhesion, traction force microscopy, and YAP/TAZ signaling, MSCs were harvested and resuspended in serum-reduced medium (DMEM with 1 v/v% FBS and 1 v/v% P/S) supplemented with 22 μg/mL AIIB2 integrin blocking antibody [Developmental Studies Hybridoma Bank, Iowa City, US] for 15 min at 25 °C. For control cell adhesion studies, MSCs were harvested and the N-cadherin function was blocked by incubating the cells with polyclonal, rabbit anti-N-cadherin antibody that specifically targets the EC1-2 domains (1:600; ProteinTech, Catalog #: 13769-1-AP) for 15 min at 25 °C before seeding. Mouse C2C12 myoblast cells (ATCC, CRL-1772) were cultured in standard myoblast growth medium containing DMEM with 4.5 g/L glucose and L-glutamine, without sodium pyruvate (Corning, Catalog #: 10-017-CV), supplemented with 20% FBS and 1% P/S. The culture media used are summarized in Suppl. Table S2.

2.8. Traction force microscopy

MSCs were seeded onto hydrogels at a density of 2.6×10^4 cells/cm^2 in serum-reduced medium supplemented with AIIB2. At 4.5 h after seeding cells onto the substrates, three images were obtained: 1) differential interference contrast (DIC) images of single cells that were separated from neighboring cells by at least one cell-width, in order to avoid mechanical interactions between cells [55], 2) fluorescent images of the beads embedded in the hydrogel just below the cell's basal plane, 3) fluorescent images of the beads in the hydrogel after removing cells from the substrate with 1 w/v% sodium dodecyl sulfate solution. All images were in the same field of view, and local drift was corrected by aligning static fluorescent beads in areas without cells. The cell boundary was manually traced from the DIC images, and the strain areas due to cell-induced deformations on the gels were constrained to the area defined by the cell boundary. The 'constrained traction forces' were calculated from the displacement fields of the fluorescent beads measured before and after cell detachment, as described [56,57]. At least 15 cells were measured per condition.

2.9. Immunofluorescence imaging of YAP/TAZ distributions and cell morphologies

MSCs were seeded on hydrogels at a density of 2.6×10^4 cells/cm^2, in reduced-serum (1%) medium containing the integrin blocking antibody AIIB2. After 5 h, the cells on the hydrogels were fixed with an acetone:methanol (1:1) solution for 20 min at −20 °C, and simultaneously permeabilized and blocked with 0.3% Triton X-100 in 1% BSA in PBS for 1 h at room temperature. The cells were first incubated overnight at 4 °C with rabbit anti-YAP (D8H1X) monoclonal antibody

(1:400 in PBS with 1% BSA, Cell Signaling Technology, Catalog #: 14,074), and then incubated with goat anti rabbit-FITC secondary antibody (1:25 in PBS with 1% BSA, ThermoFisher, Catalog #: R37116) and Alexa Fluor 657 phalloidin (F-actin stain; 1:200 in PBS with 1% BSA; Invitrogen, Catalog #: A22287) for 1 h at room temperature. Finally, the cells were incubated with 4′,6-diamindino-2-phenylindole (DAPI; 1:500 in PBS from 5 mg/mL stock in water; Invitrogen, Catalog #: D1306) for 5 min at room temperature. Between each step, the gels were rinsed with cPBS. Fluorescent images were acquired using a confocal microscope (Zeiss LSM 700, Institute for Genomic Biology, University of Illinois).

2.10. Image analysis

All image analyses (cell area, aspect ratio, circularity, and YAP/TAZ nuclear/cytosolic ratio) were performed on a single cell basis using ImageJ (NIH). At least 36 cells from random locations on three different hydrogels were used for each analysis. For each cell, the cytosolic and nuclear regions were determined by generating binary masks with a thresholding method based on the fluorescent actin and cell nucleus images. The cell area was determined from the cell mask. The aspect ratio was determined by the taking the ratio of the largest (major) and smallest (minor) width and length of the cell mask:

$$Aspect\ Ratio = \frac{Major\ Axis}{Minor\ Axis} \quad (1)$$

The cell circularity was determined from the cell mask using the following formula, where circularity ranges between 0 and 1.0, with values approaching 0 indicating an increasingly elongated shape and 1.0 indicating a perfect circle:

$$Circularity = \frac{4\pi(Area)}{(Perimeter)^2} \quad (2)$$

The ratio of nuclear to cytosolic YAP/TAZ was determined by taking the ratio of the mean fluorescence intensity of the cell nucleus, defined by the nuclear mask of the DAPI stain, and the mean fluorescence intensity of the cytosolic region, as defined by the cell mask of the actin stain. Before taking the ratio, the mean background fluorescence intensity of the surrounding areas without cells were subtracted from the mean intensities.

$$YAP/TAZ\ ratio = \frac{\text{Nuclear YAP intensity/Area of nucleus}}{\text{Cytosolic YAP intensity/Area of cytosol}} \quad (3)$$

2.11. MSC conditioned medium

MSCs were seeded at a density of 3.8×10^4 cells/cm^2 in concentrated differentiation medium (DMEM without sodium pyruvate [Corning, Catalog #: 10-017-CV] supplemented with 10% [v/v] horse serum and 1% [v/v] PS) on the hydrogel surfaces. After 6 h, the media was replaced with fresh concentrated differentiation media. At 24 h after media change, the concentrated conditioned differentiation media was centrifuged at 10,000 g for 30 min to pellet cellular debris, and the supernatant was collected. Mouse specific ELISAs for VEGF (R&D systems, Catalog #: DY493) and IGF (R&D systems. Catalog #: DY791) were used according to the manufacturer's instructions to detect paracrine concentrations in the conditioned differentiation media. For myogeneic differentiation, the supernatant was diluted at a ratio of 1:4 with DMEM without sodium pyruvate to form the differentiation media.

2.12. Myogenic differentiation in vitro

C2C12 myoblasts (passages 4–6) were seeded at a density of 2×10^4 cells per well in a tissue-cultured treated 96-well plate, and cultured in growth medium containing DMEM without sodium pyruvate and with 20% (v/v) FBS and 1% (v/v) P/S. After 24 h, the media was replaced with differentiation media and changed daily thereafter. A summary of the procedure is included in Fig. S3.

On day 5 of differentiation, the differentiated cells were fixed with 4% paraformaldehyde in PBS for 10 min, permeabilized with 0.5% Triton X-100 in PBS for 10 min and blocked with 1% BSA in PBS for 30 min, all at room temperature. Myosin heavy chain (MHC) was labeled with a mouse MF-20 antibody (1.5 μg/mL in PBS with 1% BSA; Developmental Studies Hybridoma Bank, The University of Iowa Department of Biology, US) overnight at 4 °C. Next, the cells were incubated with anti-mouse IgG Alexa Fluor 488 (1:250 in PBS with 1% BSA; Invitrogen, Catalog #: A11001) for 1 h at room temperature. Finally, 4′,6-diamindino-2-phenylindole (DAPI; 1:500 in PBS from 5 mg/mL stock in water; Invitrogen, Catalog #: D1306) was added in the dark at room temperature for 5 min to label the cell nuclei. Between each step, the cells were rinsed in PBS. The cells were imaged with a fluorescence microscope (Axio Zoom. V16, Zeiss). Myotube lengths, widths, and densities were quantified by measuring MHC-stained myotubes. Myoblast fusion index was quantified as the percentage of the number of nuclei within myotubules divided by the total number of nuclei per region of interest.

Separately, on day 5 of differentiation, the cells were lysed with RIPA lysis and extraction buffer (Thermo Scientific, Catalog #: 89,901) for 5 min at 4 °C, sonicated for 15 s, and centrifuged at 10,000 g for 15 min to remove cell debris. A liquid creatine kinase reagent kit was used according to manufacturer's instructions to measure creatine kinase activity (Pointe Scientific, Catalog #: C7522). Changes in absorbance due to creatine kinase activity was detected using a fluorescent plate reader at 340 nm.

2.13. Isolation and modification of red blood cells (RBCs) with N-cadherin ligands

The N-cadherin ligands were immobilized and oriented on the surfaces of human red blood cells (RBCs) for measurements of the protein binding affinities, using adhesion frequency measurements (Suppl. Fig. S3). Whole blood was collected from healthy volunteers at Community Blood Services of Illinois (CBSI), and red blood cells were isolated and purified from whole blood (IRB; Protocol #: 08669), as previously described [52].

Anti-mouse IgG Fc (1:200; Sigma Aldrich, Catalog #: M4280) was covalently immobilized on RBC surfaces, to capture Fc-tagged N-cad EC1-5. Streptavidin was immobilized on RBCs to capture biotinylated N-cad EC1-2 or biotinylated HAVDI-containing peptide. These capture proteins were covalently bound to the RBCs, following chromium (III) chloride ($CrCl_3$) activation, as previously described [58,59]. The density of the immobilized 'capture protein' was controlled by titrating the $CrCl_3$ concentration used to activate the RBCs. Approximately 10^6 RBCs were rinsed five times with 0.85 w/v% NaCl, and then resuspended in 0.85 w/v% NaCl with 10 μg/mL of the capture protein. Separately, serial dilutions of $CrCl_3$ were prepared from 0.1 (v/v) % $CrCl_3$ solution in 0.02 mM sodium acetate and 0.9% (w/v) NaCl. The RBC/capture protein was mixed in a 1:1 ratio with the $CrCl_3$ solution for 5 min, and the reaction was halted by rinsing the cells with PBS containing 5 mM EDTA and 1 w/v% BSA. The cells were suspended and stored in EAS 45 buffer at 4 °C until use. On the day of the micropipette aspiration assay measurements, N-cadherin fragments (1 mg/mL) were added to the functionalized RBCs at a final dilution of 1:12 for 45 min at 4 °C.

2.14. Quantification of N-cadherin densities on MSCs and RBCs

The densities of expressed N-cadherin on MSCs or immobilized N-cad EC1-5 and N-cad EC1-2 on RBC surfaces were quantified by flow cytometry, as previously described [49,60]. MSCs and RBCs displaying N-cad EC1-5 or N-cad EC1-2 were labeled for 45 min with a rabbit, anti-N-cadherin polyclonal antibody that specifically binds to the EC1-2 domain (1:600 in cPBS with 2% BSA, ProteinTech, Catalog #: 13769-1-

AP). After, the cells were incubated with secondary Cy5™ goat anti-rabbit antibody (1:400 in PBS with 0.9 mM calcium; Invitrogen, Catalog #: A-21245) for 45 min. The cells were washed twice with PBS before and after the incubation with the secondary antibody, in order to remove the unbound, excess antibodies. The fluorescence intensity of labeled cells and of the standardized calibration beads for Alexa 647 (Bangs Laboratories, Inc., IN) were quantified using an LSR II flow cytometer (BD Biosciences, San Jose, CA). The fluorescence intensities were converted to total cadherin densities on the cells, by comparing the fluorescence with the calibration curves, according to the manufacturer's instructions [60]. The cadherin densities were further confirmed by using a primary, rabbit anti-monoclonal N-cadherin antibody (1:200 in PBS with 0.9 mM calcium; Abcam, Catalog #: ab76011, Cambridge, MA), which recognizes the EC1 domain of N-cadherin, for 45 min.

To determine the surface density of biotinylated HAVDI peptides, the RBCs were labeled with streptavidin Alexa 647 conjugate (1:400; Thermo Fisher, Catalog #: S21374). Before flow cytometry, the biotinylated HAVDI peptides were incubated with ~400,000 streptavidin-modified cells for 45 min at 4 °C. Quantitative comparisons of the density of N-cad EC1-2 on RBCs modified with unlabeled streptavidin to the density of immobilized streptavidin-fluorophore conjugate on RBCs modified under otherwise identical conditions showed that the stoichiometry of biotinylated N-cad EC1-2 or biotinylated peptide to streptavidin was 2:1.

2.15. Micropipette aspiration measurements of protein binding kinetics

Affinities determine cadherin adhesion, so any differences in ligand affinities would identify potential differences in cell adhesion to surfaces modified with the different proteins or peptides at similar surface density. To do this, we used micropipette measurements to compare the binding affinities between each of the different N-cadherin ligands immobilized on red blood cells (RBCs) and N-cadherin expressed on MSCs. We also compared binding affinities between the different ligands immobilized on RBCs. RBCs were used as they can be easily modified with different proteins. In addition, they also have a soft, smooth membrane that easily deforms when the cells are pulled apart. The deformation can be used to determine binding events. Micropipette adhesion frequency measurements [60] quantify cadherin affinities based on the time-dependent binding probability between MSCs and red blood cells (RBCs) displaying N-cadherin EC1-5, N-cadherin EC1-2, or peptides. In the micropipette measurements, the MSC (or test cell) is held in one micropipette and another cell (RBC or MSC) is held in the opposing micropipette. The cells are brought into contact with a programmable piezo-electric controller for a definite period (0.5 s–40s), and then separated. We record the time dependent binding probability, which is the number of detected cell-cell adhesion events, n_b divided by the total number of cell-cell touches, N_T, or $P = n_b/N_T$. The probability is a function of the number of intercellular bonds that form during a defined cell-cell contact time. Throughout the experiment, the cells were kept in a hypotonic Leibovitz's L-15 Medium (Invitrogen, Carlsbad, CA) containing 2.0 mM $CaCl_2$ diluted 1:1 with deionized water to maintain a rounded form. Cells were observed with a 100× oil immersion objective on a Zeiss Axiovert 200 microscope, interfaced with CCD camera (Pike, Allied Vision Technologies), and the contact area was controlled at ~ 7 μm^2.

The binding kinetics between N-cadherin proteins or peptides were determined from the measured adhesion frequency between a soft, cadherin-modified RBC and a second test cell. For each contact time, three different cell pairs were subjected to 50 cell-cell contacts ($N_T = 50$). Values of the probability at each time point are reported as the average ± standard deviation.

The adhesion probability (P) was measured from the running frequency of binding events for receptor-ligand pairs (150 measurements per contact duration). The dissociation rate and steady state, two-dimensional affinities were estimated from model fits to plots of the adhesion probability versus contact duration. The model used to evaluate the binding interaction was based on McQuarrie's probabilistic formulation of kinetics in small systems [61]. For a simple second order binding reaction A + B → C, the analytical solution of the master equations derived by Chesla et al. [60] describes the time-dependence of the adhesion probability:

$$P_a = 1 - \exp\{-A_c\, m_r m_l K_a [1 - \exp(-k_{off}\, t)]\} \quad (4)$$

where A_c is the contact area (μm^2), m_r and m_l are cadherin densities on the two cells (number/μm^2), K_a is the two-dimensional affinity (μm^2), and k_{off} is the dissociation rate (seconds).

The measured time-dependent adhesion probability was fit to Eqn. (4), using the Levenberg-Marquardt nonlinear, least squares regression in the OriginLab software package (Northampton, MA). The best, unbiased estimated parameter is determined by weighted, non-linear least squares analysis, with the weighting factor for each time point being the inverse of the variance at that time point. A non-linear lack-of-fit test identified the time points that are associated with the first, EC1 dependent binding step (strand swapped dimer) [62]. The test compares the model's residuals to the inherent variability in the data, normalized to an F-distribution, as previously described [63], and a student's t-test was performed to determine statistical significance between measured 2D affinities.

3. Results

3.1. Displaying N-cadherin ligands on hydrogels for cell adhesion

The acrylamide monomer and bis-acrylamide crosslinker concentrations were adjusted to form polyacrylamide hydrogels with elastic moduli of 10 and 36 kPa, which correspond to the physiological stiffness of muscle and osteoid, respectively [64,65]. The different N-cadherin fragments N-cad EC1-5-Fc or N-cad EC1-2-biotin were captured and oriented on Protein A or Neutravidin that were covalently immobilized on the hydrogels, respectively (Fig. 1b). The densities of the N-cadherin fragments or peptides on the gels were quantified by ELISA or fluorescence, respectively. Immobilization conditions were tuned to yield densities of $4.5 \pm 0.6 \times 10^{-11}$ mol/cm^2 for cadherin fragments or peptides used.

The studies used three different immobilization strategies. However, results reported here and in prior studies confirmed that cell surface N-cadherin binds to the immobilized ligands in all three contexts (Fig. 1c). Cells adhere to Fc-tagged cadherin extracellular domains immobilized on protein A (or anti-Fc antibody) and activate characteristic cadherin-mediated signaling [66]. Physisorbed EC1-2 fragments support cadherin-dependent cell adhesion [48]. Here, immobilized biotinylated N-cad EC1-2 on Neutravidin in order to ensure that the binding site is oriented towards cadherin on adjacent cells, as with the Fc-tagged extracellular domain. Similar to prior studies, cells also adhered to peptides directly coupled to the hydrogels [21,25].

The MSCs adhered to hydrogels modified with N-cad EC1-5, N-cad EC1-2, or HAVDI (Fig. 1c), but not to the control, scrambled peptide. Cell treatment with an N-cadherin blocking antibody targeting the EC1-2 domain decreased cell attachment by 90%, confirming the cadherin-specific cell adhesion. In addition, there was negligible cell adhesion on polyacrylamide substrates with only Protein A or neutravidin. Conversely, treating cells with N-cadherin blocking antibody prior to seeding cells on type I collagen-modified hydrogels had no effect on cell adhesion (Suppl. Fig. S4). The densities of MSCs adhered to gels modified with any of the three N-cadherin fragments were not statistically different, after 24 h in culture (Fig. 1c).

3.2. MSC spreading depends on the N-cadherin fragment

The results of the determined spreading of the MSCs on the modified

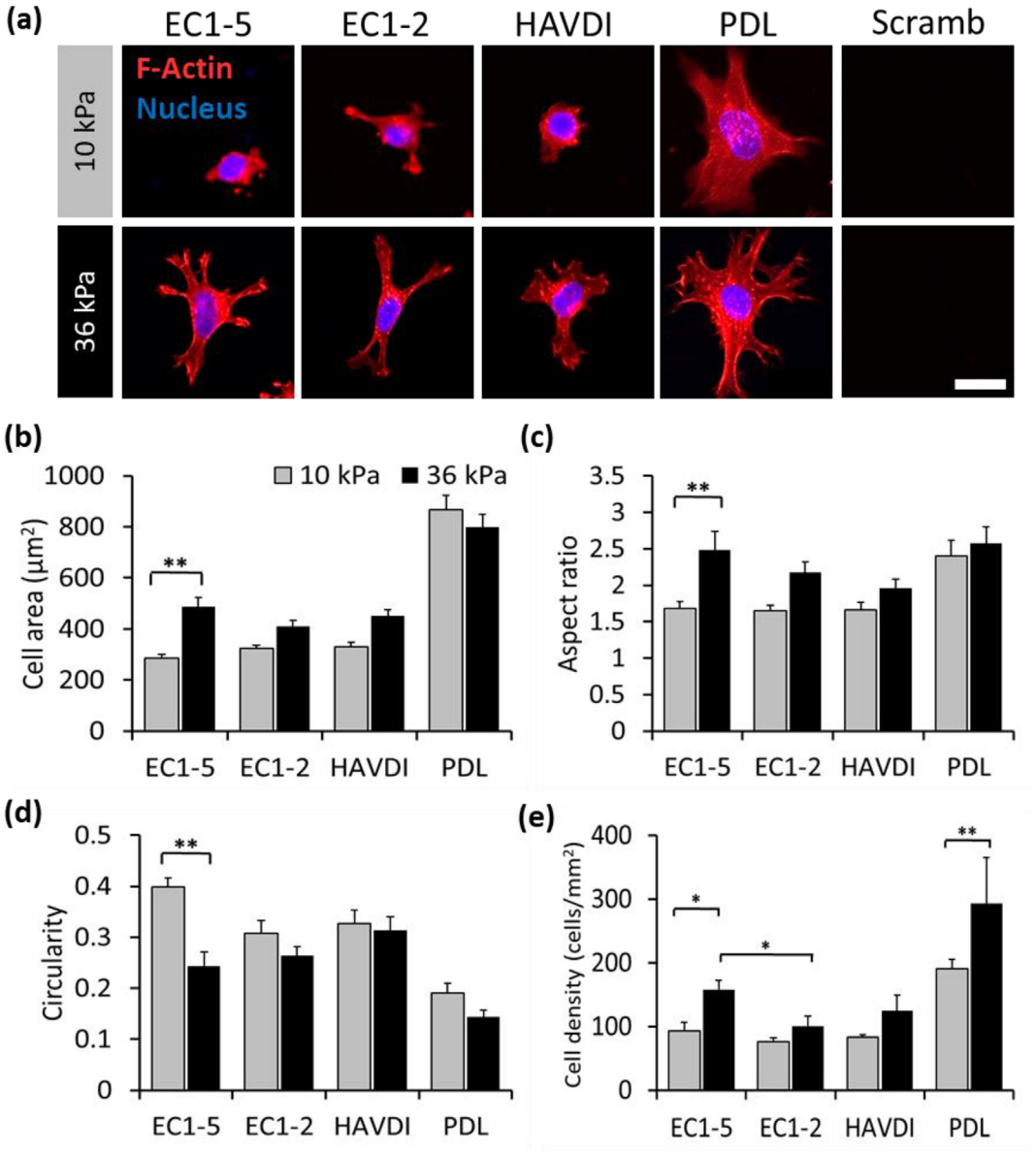

Figure 2. Dependence of cell morphology and attachment densities on soft versus stiff gels coated with different N-cadherin ligands. (a) Representative F-actin (red) and nuclear (blue) staining of MSCs cultured on top of hydrogels with different immobilized proteins and peptides (N-cadherin EC1-5, EC1-2, HAVDI, poly-*d*-lysine or PDL, and scrambled peptide), and elastic modulus (10 and 36 kPa). Scale bar represents 20 μm. Corresponding quantification of (b) spread area, (c) aspect ratio, and (d) circularity. ($n \geq 36$ cells per condition for a-d; **: $p < 0.01$; two-way ANOVA with Tukey-HSD post-hoc; mean +s. e.m.). (e) Cell density of MSCs adhered onto hydrogel surfaces. ($n \geq 9$ area on hydrogels per condition; *: $p < 0.05$; **: $p < 0.01$; one-way ANOVA with Tukey-HSD post-hoc; mean ± s. e.m.).

hydrogels are shown in Fig. 2. The elastic modulus affected the cell area, aspect ratio, and circularity of MSCs cultured on N-cad EC1-5. Specifically, MSCs cultured on 10 kPa hydrogels coated with N-cad EC1-5 exhibited lower spread areas and aspect ratios, but increased circularity, compared to MSCs on 36 kPa hydrogels. In contrast, on N-cad EC1-2 conjugated hydrogels, the modulus did not affect the cell area, aspect ratio, or circularity, within experimental error. Also, the substrate modulus affected the average spread area of cells on HAVDI substrates, but not the aspect ratio or the circularity, within error. However, there was no statistical difference between the aspect ratio, circularity, and cell density of MSCs cultured on N-cad EC1-2 or HAVDI modified hydrogels with moduli of 10 kPa versus 36 kPa. MSCs cultured on poly-*d*-lysine (PDL) exhibited significantly higher cell area, decreased circularity, and increased cell density (Fig. 2). The densities of attached cells (Fig. 2e) appeared to be relatively insensitive to substrate rigidity, although on 36 kPa gels, more cells adhered to hydrogels coated with N-cad EC1-5, relative to the other fragments. However, despite some individual differences, there were no fragment-specific trends in cell attachment or spreading on the compliant gels.

3.3. Different N-cadherin ligands support similar rigidity-dependent cell traction

Traction force microscopy quantified cadherin-mediated MSC traction generation 5 h after seeding the cells. Fig. 3 compares the traction forces generated by MSCs on polyacrylamide hydrogels with elastic moduli of 10 kPa and 36 kPa, when modified with similar densities ($4.5 \pm 0.6 \times 10^{-11}$ mol/cm^2) of N-cad EC1-5, N-cad EC1-2, or HAVDI. The N-cadherin-mediated traction forces depended on the elastic modulus, as the decrease in the elastic modulus from 36 kPa to 10 kPa reduced the root mean square traction forces by ~75% in all cases. The MSCs exhibited similar stiffness-dependent traction forces

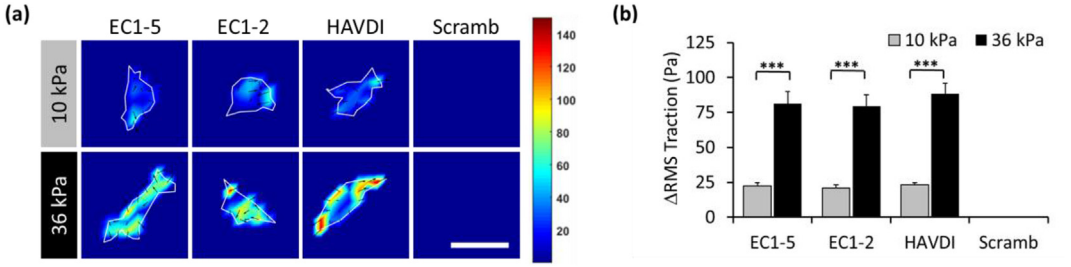

Fig. 3. Traction forces exerted by MSCs. (a) Representative heat maps of traction forces exerted by MSCs on 10 kPa or 36 kPa hydrogels modified with N-cad EC1-5, N-cad EC1-2, HAVDI, or the scrambled peptide. Scale bar represents 30 μm. The heat map represents local traction force (Pa). (b) Quantification of the constrained root-mean-square (RMS) traction forces (Pa) exerted by MSCs represented in part (a). Modified substrates had elastic moduli of 10 kPa (grey) or 36 kPa (black). ($n > 16$ cells per condition; ***: $p < 0.001$; two-way ANOVA with Tukey-HSD post-hoc; mean ± s. e.m.).

when cultured on hydrogels modified with any of the three N-cadherin fragments studied here.

3.4. YAP/TAZ nuclear translocation

We next determined whether kinetic and affinity differences between N-cadherin fragments differentially affected downstream mechanosensitive signaling pathways. The *Yorkie*-homologues YAP (yes-associated protein) and TAZ (transcriptional co-activator with PDZ-binding motif) were used as nuclear relays of signals exerted by the cells in response to mechanical cues. The YAP/TAZ nuclear localization for MSCs cultured on hydrogels with elastic moduli of 10 kPa and conjugated with either N-cad EC1-5 or N-cad EC1-2 were similar (Fig. 4). In both cases, the YAP/TAZ nuclear localization was higher on the 36 kPa hydrogels. However, with MSCs cultured on HAVDI conjugated hydrogels, there was no statistically significant, rigidity-dependence of the nuclear/cytosolic YAP/TAZ ratios (Fig. 4). Moreover, YAP/TAZ localization was similar in MSCs cultured on 36 kPa hydrogels modified with either N-cad EC1-5 or N-cad EC1-2. In controls, MSCs cultured on PDL coated 36 kPa hydrogels showed higher YAP/TAZ nuclear localization compared to the N-cadherin coated surfaces.

3.5. Paracrine secretion depends on the N-cadherin fragment

After 24 h of culture, an ELISA assay was used to determine the concentrations of vascular endothelial growth factor (VEGF) and insulin-like growth factor 1 (IGF-1) in the conditioned medium from the MSCs cultured on hydrogels modified with different N-cad fragments. Both VEGF and IGF-1 are key regulators of skeletal muscle differentiation [67–70]. The secreted VEGF (Fig. 5a) and IGF-1 (Fig. 5b) were normalized to the total number of cells seeded per area, in order to exclude the possibility that different growth rates between MSCs grown on the different hydrogels might bias the secretion level. In addition, serum-containing medium was used, instead of the serum-reduced medium with integrin antibodies used elsewhere in this study, in order to support the longer culture time and subsequent use of the conditioned medium for future myogenic differentiation studies.

The results in Fig. 5a and b showed that MSCs cultured on N-cadherin EC1-5 immobilized on hydrogels secreted at least 20% higher levels of VEGF and IGF-1 than MSCs cultured on either N-cadherin EC1-2 or HAVDI, regardless of the elastic modulus of the substrate. IGF-1 secretion levels were similar for MSCs cultured on hydrogels immobilized with N-cadherin EC1-2, HAVDI, and the scrambled peptide, regardless of elastic moduli. However, VEGF secretion was higher on hydrogels immobilized with N-cadherin EC1-2 than with HAVDI or the scrambled peptide, regardless of elastic moduli. MSCs on hydrogels immobilized with either HAVDI or the scrambled peptide secreted the lowest concentrations of VEGF and IGF-1. Overall, the results observed with MSCs cultured on hydrogels immobilized with N-cad EC1-5 agree with previous reports that N-cadherin expression and N-cadherin mediated interactions in cell clusters correlates with increased VEGF and IGF-1 secretion by MSCs [22,23].

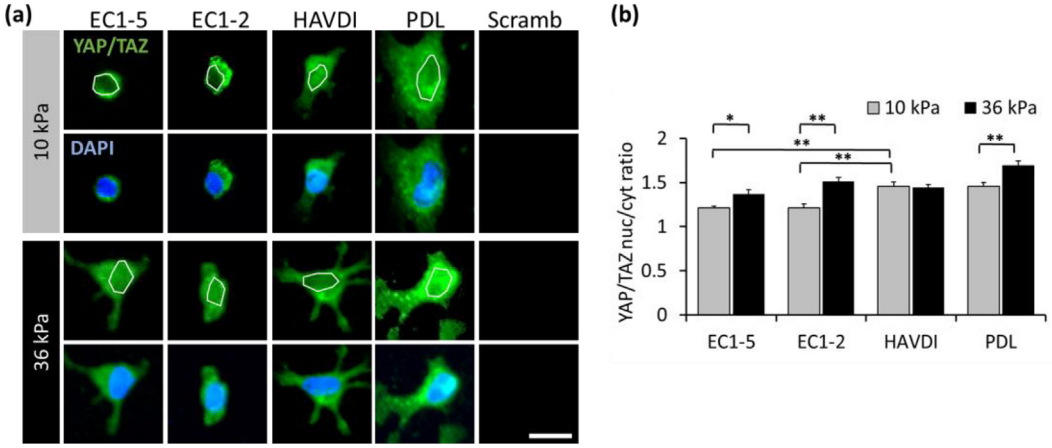

Fig. 4. N-cadherin fragments influence YAP/TAZ nuclear localization. (a) Representative confocal images of YAP/TAZ (green) and DAPI (blue) in MSCs cultured on hydrogels with different immobilized proteins and peptides (N-cadherin EC1-5, EC1-2, HAVDI, PDL, and scrambled peptide), and with different elastic moduli (10 and 36 kPa). The solid white lines outline the nuclei (blue), as observed in the merged images. The scale bar represents 20 μm. (b) Quantification of YAP/TAZ nuclear to cytoplasmic ratios for each group represented in part (a). Modified substrates had elastic moduli of 10 kPa (grey) or 36 kPa (black). ($n > 36$ cells per condition; *: $p < 0.05$; two-way ANOVA with Tukey-HSD post-hoc; mean ± s. e.m.). (For interpretation of the references to colour in this figure legend, the reader is referred to the Web version of this article.)

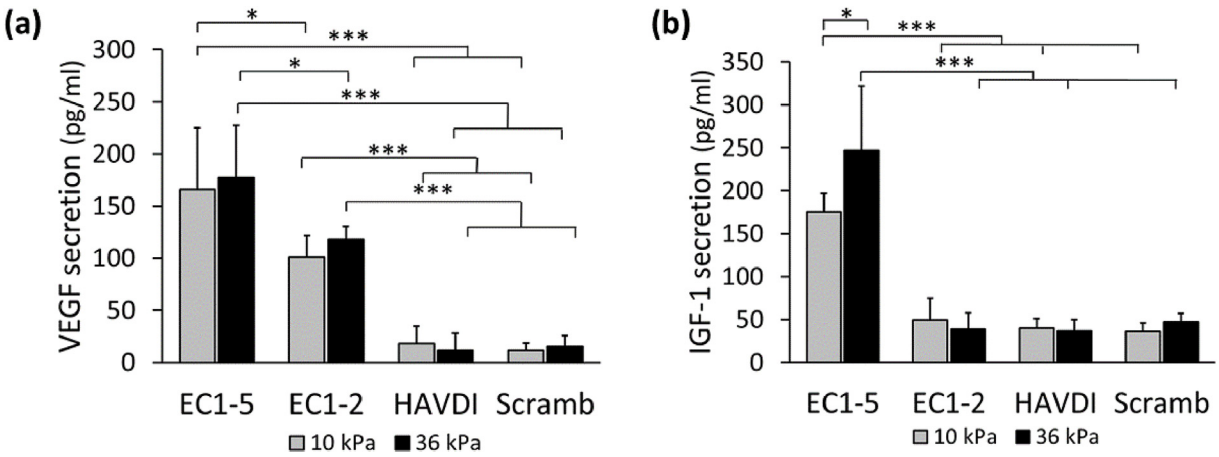

Fig. 5. VEGF and IGF-1 secretion depends on specific N-cadherin fragments. Secretion of (a) VEGF and (b) IGF-1 by MSCs (with an initial seeding density of 3×10^4 cells) cultured on hydrogels conjugated with the different proteins and peptides. Modified hydrogels had elastic moduli of 10 kPa (grey) or 36 kPa (black) (n = 5 gels per condition; *: $p < 0.05$; ***: $p < 0.001$; two-way ANOVA with Tukey-HSD post-hoc; mean ± s.d.).

3.6. MSC-conditioned medium induces myogenic differentiation

To assess the impact of paracrine secretion on myogenesis, MSC-conditioned differentiation medium was added to the C2C12 myoblast culture (Suppl. Fig. S3). The morphology of the differentiated C2C12 cells was then characterized by the width, length, area, and fusion index of myosin heavy chain (MHC)-positive myotubes, as indicators of the maturity of the differentiated myotubes (Fig. 6a). The myotube widths (Fig. 6b), lengths (Fig. 6c), and fusion index (Fig. 6d) were all higher for the C2C12s cultured in conditioned differentiation medium from MSCs cultured on N-cad EC1-5, compared to MSCs cultured on the scrambled peptide control, regardless of substrate stiffness. Differences between myotube widths, lengths, and fusion indices of cells on N-cad EC1-2 or N-cad EC1-5 on 10 kPa hydrogels were not statistically significant; however, the myotube width and fusion index were different for the 36 kPa hydrogels. The C2C12s cultured with conditioned differentiation medium from MSCs cultured on HAVDI or scrambled peptide were similar to each other, regardless of the stiffness of MSC substrates. There was also no significant difference between the myotube lengths, diameters, and fusion indices, between the two stiffnesses for MSCs cultured on either N-cad EC1-2 or HAVDI.

In addition, the production of muscle creatine kinase levels, which is a quantitative gauge of myogenesis in mature skeletal muscle [71,72] was substantially higher in C2C12s that were cultured in MSC-CDM from MSCs cultured on N-cad EC1-5 modified 36 kPa gels, compared to all other conditions (Fig. 7). Minimal differences were observed for C2C12s grown in MSC-CDM from MSCs on the other N-cad fragments, regardless of substrate stiffnesses. In controls in which the C2C12s were cultured in growth medium as opposed to differentiation medium, muscle creatine kinase levels were 50-fold lower.

3.7. N-cadherin binding affinities

To identify biophysical differences between the fragments that might account for differences in cell spreading, YAP/TAZ translocation, and paracrine secretion, we quantified the binding affinities between each of the different N-cadherin ligands immobilized on red blood cells (RBCs) and N-cadherin expressed on MSCs. Specifically, the goal of these binding affinity measurements was to i) demonstrate that the immobilized N-cadherin ligands bind to N-cadherin expressed on MSCs, ii) compare the binding affinities of N-cadherin ligands to each other and to N-cadherin on MSCs, and iii) quantify potential binding of N-cadherin to E-cadherin, which is also expressed on MSCs and could thus confound results attributed to N-cadherin. Measurements between two RBCs displaying N-cadherin ligands quantified the N-cadherin-explicit binding affinities, independent of potential interactions with cell surface proteins such as E-cadherin. Measurements between the ligand-displaying RBCs and MSCs in turn quantified differences in ligand affinities for cell-surface N-cadherin.

Micropipette adhesion frequency measurements were used to quantify the two-dimensional binding affinities (Fig. 8a) [49,52,66,73]. The binding probability versus cell-cell contact time measured between N-cad EC1-5 ligands on RBCs and other N-cadherin ligands on opposing RBCs are presented in Fig. 8b. The binding probability versus cell-cell contact time measured between N-cad EC1-5 ligands exhibited a two-stage kinetic signature (Fig. 8b), which is characteristic of type I classical cadherins studied to date [49,52,66,73]. Namely, there was a rapid rise to an initial plateau at P~0.32, followed by a brief lag, and then a second increase in binding probability to a final steady-state plateau at P~0.45. Prior studies with domain deletion mutants verified that the initial binding step reflects the formation of a strand swapped dimer between EC1 domains [49]. The second increase requires the EC3 domain [49], and correlates with the ability to form cadherin clusters at cell-cell junctions [51]. Consistent with prior findings, the kinetics measured between N-cadherin EC1-5 and either N-cadherin EC1-2 or HAVDI, which both lack EC3, exhibited a monotonic rise to a single plateau (Fig. 8b) [49].

To determine the EC1-EC1 binding affinity (Fig. 1a), analyses focused on the fast, first binding step [49]. The 'strand swap' binding mechanism is described by a second order rate equation (Eq. (4)). In measurements between EC1-5 fragments, a non-linear lack-of-fit test identified the time points associated with the first, EC1-dependent binding step [62]. For kinetic data that exhibited a single monotonic increase, all data points were used in the fits (see Methods). Importantly, differences in the amplitudes of the initial plateaus are due, in part, to differences in cadherin densities on the cells. Differences in cadherin surface densities were accounted for by the fixed (measured) parameters m_L and m_R Eq. (4).

The best-fit, two-dimensional (2D) binding affinities determined for different pairwise ligand interactions are summarized in Table 1 and Suppl. Table S3. The 2D affinity between N-cad EC1-5 fragments was $14.8 \pm 0.4 \times 10^{-5}$ μm^2. Binding between EC1-5 and EC1-2 did not exhibit two-stage binding kinetics, and the best fit affinity was $7.5 \pm 0.1 \times 10^{-5}$ μm^2, which is significantly less than between N-cad EC1-5 ($p < 0.05$, n = 3). N-cad EC1-5 also binds HAVDI with an affinity of $7.9 \pm 0.1 \times 10^{-5}$ μm^2. The latter was similar to the affinity between N-cad EC1-5 and N-cad EC1-2 ($p > 0.05$, n = 3), but ~2 fold lower than that between N-cad EC1-5 fragments. Other pairwise ligand binding affinities are included in Suppl. Fig. S5 and Table S3. The scrambled peptide binds non-specifically to RBCs modified with either

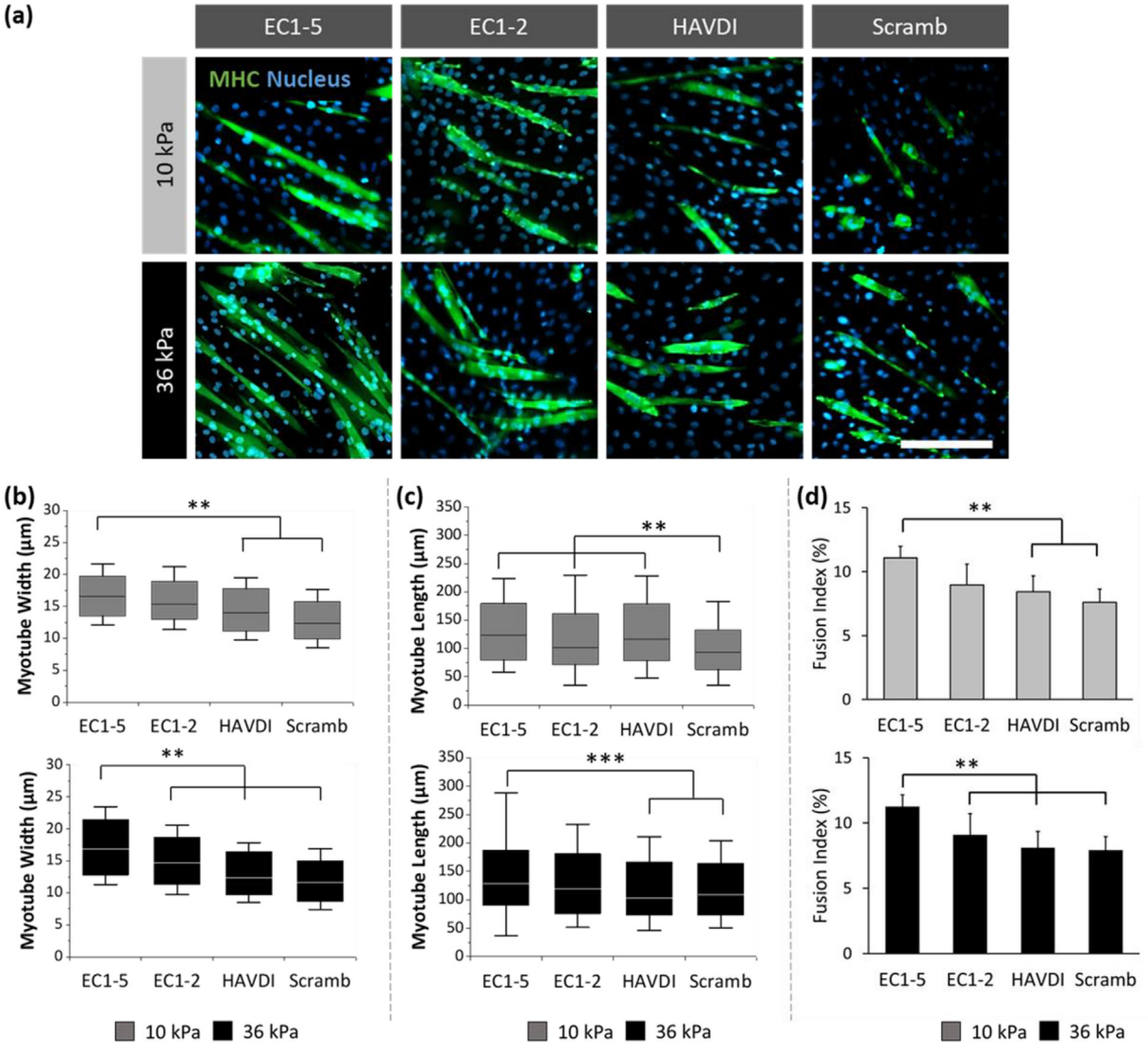

Fig. 6. Conditioned media from MSCs cultured on N-cadherin fragments improves myogenic differentiation. (a) Representative immunofluorescent images of differentiated myoblasts stained for myosin heavy chain (MHC, green) and the cell nucleus (DAPI, blue). Scale bar represents 100 μm. (b) Mean myotube width. Myotubes were cultured in conditioned differentiation medium from MSCs grown on gels with N-cad fragments and either an elastic modulus of 10 kPa (grey) or 36 kPa (black). ($n > 200$ per condition; **: $p < 0.01$; one-way ANOVA with Tukey's post-hoc test; box plots show 25/50/75th percentiles, whiskers show minimum/maximum). (c) Mean myotube length. Myotubes were cultured in conditioned differentiation medium from MSCs grown on gels with N-cad fragments and either an elastic modulus of 10 kPa (grey) or 36 kPa (black). ($n > 200$ per condition; **: $p < 0.01$, ***: $p < 0.001$; one-way ANOVA with Tukey's post-hoc test; box plots show 25/50/75th percentiles, whiskers show minimum/maximum). (d) Mean fusion index. Myotubes were cultured in conditioned differentiation medium from MSCs grown on gels with N-cad fragments and either an elastic modulus of 10 kPa (grey) or 36 kPa (black). ($n \geq 5$ per condition; **: $p < 0.01$, one-way ANOVA with Tukey's post-hoc test; bar graphs show mean ± s.d.). (For interpretation of the references to colour in this figure legend, the reader is referred to the Web version of this article.)

N-cad EC1-5, N-cad EC1-2, or HAVDI (Suppl. Fig. S6). In addition, the HAVDI peptides do not bind to each other (Suppl. Fig. S6).

Next, we quantified the binding kinetics between N-cadherin expressed on MSCs and the N-cadherin ligands on an opposing RBC (Fig. 8c). N-cad EC1-5 binding to MSCs also exhibited two-stage kinetics. The determined EC1-EC1 binding affinity of $14.0 \pm 0.1 \times 10^{-5}$ μm^2 was statistically similar to that between identical N-cad EC1-5 ligands ($p > 0.05$, $n = 3$). Likewise, the time-dependent binding probabilities measured between MSCs and either N-cad EC1-2 or HAVDI exhibited a monotonic rise to a limiting plateau, and the best fit affinities were $7.3 \pm 0.2 \times 10^{-5}$ μm^2 and $7.95 \pm 0.02 \times 10^{-5}$ μm^2, respectively. These results are summarized in Table 1.

MSCs also express E-cadherin at ~7 ± 3 cadherin/μm^2 ($n = 7$). Because E-cadherin also binds N-cadherin [46,66,74], control measurements blocked E-cadherin on MSCs with the anti-E-cadherin antibody DECMA-1. This treatment did not significantly affect the affinity measured between MSCs and either N-cad EC1-5 or HAVDI (Suppl. Fig. S7 and Suppl. Table S4). Also, E-cad EC1-5 binds HAVDI with a much lower affinity ($1.51 \pm 0.06 \times 10^{-5}$ μm^2) than N-cad EC1-5 ($7.9 \pm 0.1 \times 10^{-5}$ μm^2) ($p < 0.05$, $n = 3$) (Suppl. Fig. S8 and Suppl. Table S5), in agreement with previous findings [42]. Thus, E-cadherin expressed on MSCs should not contribute significantly to MSC binding to substrates displaying the different N-cadherin ligands.

4. Discussion

This study quantified binding differences between three different N-cadherin-mimetic ligands. Although the binding differences did not result in differences in N-cadherin mediated MSC attachment,

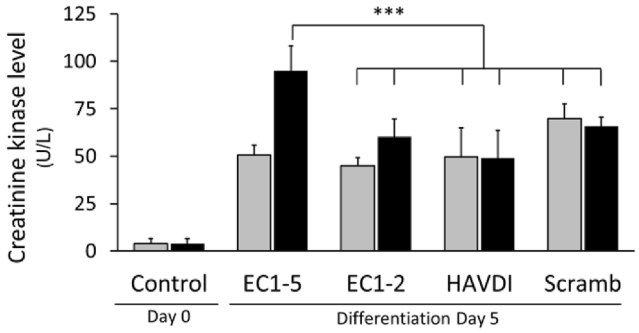

Fig. 7. N-cadherinligands affect mean creatine kinase levels. Myotubes were cultured in conditioned differentiation medium from MSCs grown on gels displaying either of the N-cad fragments. The gels had an elastic modulus of 10 kPa (grey) or 36 kPa (black). (n = 3 per condition; ***: $p < 0.001$; two-way ANOVA with Tukey's post-hoc test; mean ± s.d.).

spreading, and traction generation, they did correlate with differences in signaling and paracrine secretion. We used micropipette measurements to quantify differences in the affinities and kinetics of binding between MSCs and N-cad EC1-5, N-cad EC1-2, and HAVDI-containing peptide. The binding affinity of Fc-tagged N-cad EC1-5 on RBCs is quantitatively similar to wild-type N-cadherin on MSCs. This result confirms that binding by Fc-tagged N-cad EC1-5 is quantitatively and mechanistically similar to N-cadherin on the cell surface. However, the binding kinetics of either N-cad EC1-2 or HAVDI peptide are qualitatively and quantitatively different from N-cad-EC1-5. Both have significantly lower affinities for N-cadherin on MSCs than the full-length extracellular domain.

It is important to address the use of different immobilization strategies and their potential impact on the outcomes. The direct conjugation of the HAVDI peptide to hydrogels through the 10th amino acid from the N-terminus is the same conjugation used in several reports [21,24,35]and is therefore appropriate for functional comparisons with the other ligands. The thus immobilized HAVDI peptide is accessible to N-cadherin on the cell surface, as confirmed in controls with scrambled peptide and with N-cadherin blocking antibodies. The long tether used to immobilize the biotinylated peptides on streptavidin in affinity measurements also insures peptide accessibility, as confirmed in controls with scrambled peptide. We also show that binding by N-cad EC1-5-Fc immobilized to RBCs via protein A is quantitatively similar to N-cadherin on MSCs (Table 1); this immobilization strategy does not impair the protein function. The lower affinity of the N-cad EC1-2 ligand is consistent with a prior report [49] and with findings that mutations at the EC2-EC3 junction can impair cadherin adhesion [75,76]. The measurements thus reflect ligand binding in the contexts in which they are used in biomaterials [21,24,28,30] and in cell biology studies of N-cadherin adhesion [29,66,77].

Affinities determine cadherin-mediated cell adhesion strengths. However, the differences in ligand-cadherin binding affinities did not result in any clear correlations with either cell spreading or traction force generation under serum-reduced conditions. The N-cad EC1-5 exhibits the highest *trans*-binding affinity for cell-surface N-cadherin relative to either of the other cadherin ligands investigated. N-cad EC1-5 appeared to support slightly greater cell attachment efficiency and spreading than N-cad EC1-2. The lack of obvious correlations between affinity and circularity or aspect ratio, may be due to the irregular shapes of the MSCs that could mask differences.

It is somewhat surprising that the two-fold affinity differences between N-cad EC1-5 versus the other two N-cadherin ligands did not detectably affect traction force generation. However, spreading and traction generation depend on N-cadherin dependent signaling, which can involve cross-talk with other cell surface proteins such as growth factor receptors [77,78]. Thus, other cellular factors as well as growth factors in the culture medium could account for the traction force data reported here. Although there were no detectable differences between traction forces exerted on these ligands when cultured on gels with the same modulus, the tractions were rigidity-dependent in all three cases.

Despite the lack of apparent correlations between affinities and spreading or traction generation, the N-cadherin ligands elicited differences in YAP/TAZ nuclear localization and paracrine secretion, when comparing cells on hydrogels of the same elastic modulus. N-cad EC1-5, which has the highest affinity to MSCs, supports stiffness-dependent changes in YAP/TAZ nuclear localization and greater VEGF and IGF-1 secretion, relative to the other ligands. However, the differences may not be due solely to affinity differences. N-cad EC1-2 and HAVDI bind MSCs with similar affinities and appear to elicit similar IGF-1 secretion. However, on 10 kPa hydrogels, nuclear levels of YAP/TAZ exceeded those in cells on HAVDI, compared with both N-cad EC1-5 and N-cad EC1-2. YAP/TAZ localization was similar in cells adhered to the latter two proteins, despite their two-fold affinity differences. On 36 kPa gels, the nuclear/cytoplasm YAP/TAZ ratios were independent of the immobilized N-cadherin ligand. It is important to point out that there is currently no established relationship between the nuclear accumulation of YAP/TAZ and paracrine secretion; these readouts merely reflect cell responses to the environment.

Previous reports documented increases in paracrine secretion by MSCs associated with N-cadherin mediated cell-cell interactions [22]. Of these paracrine factors, both VEGF and IGF-1 are key regulators of skeletal muscle differentiation [67–70]. Here, MSCs on hydrogels immobilized with N-cad EC1-5 secreted higher levels of VEGF and IGF-1, compared to all other conditions investigated. However, there was no increase in paracrine secretion of VEGF and IGF-1 by MSCs cultured on hydrogels immobilized with HAVDI compared to the control conditions. The increase in secreted factors from MSCs cultured on N-cad EC1-5 likely contributed to the enhanced myogenic differentiation of C2C12s, apparent in the longer and wider myotubes formed, and the increased fusion of cells to form the myotubes. Previous papers similarly reported that higher VEGF and IGF-1 concentrations enhanced myogenic differentiation [67–70]. Additionally, our results suggest that IGF-1, which was secreted at higher levels by MSCs grown on 36 kPa gels immobilized with N-cad EC1-5, may result in higher muscle creatine kinase levels.

These findings show that several features of MSCs cultured on N-cadherin fragments depend on substrate rigidity. Traction generation, YAP/TAZ localization, and paracrine secretion all depended on substrate rigidity, except for the nuclear accumulation of YAP/TAZ in MSCs on HAVDI. The latter result differs from the rigidity-dependence of YAP/TAZ localization reported by Cosgrove and coworkers, but this may be due to the different experimental conditions used [21]. Previously, the nuclear/cytoplasmic ratios of YAP/TAZ were determined in cells cultured on substrates modified with mixtures of RGD (arginine-glycine-aspartic acid, a peptide that mimics integrin interactions) and HAVDI-containing peptide, in serum-containing medium without the inclusion of integrin-function blocking antibodies. Here, only N-cadherin fragments were immobilized on the gels, and the use of integrin function-blocking antibodies and low serum conditions impeded integrin dependent signaling. This approach therefore isolated N-cadherin mediated effects.

5. Conclusions

These results quantified biophysical and biochemical differences between the different N-cadherin fragments and demonstrated the response of MSCs to the different fragments with regards to cell adhesion, YAP/TAZ translocation to the nucleus, and paracrine secretion. The findings show that the full-length extracellular domain, N-cad EC1-5, has the greatest impact on stiffness-dependent changes in the nuclear localization of YAP/TAZ, paracrine secretion, and the effects of the MSC conditioned medium on myogenic differentiation. There is no

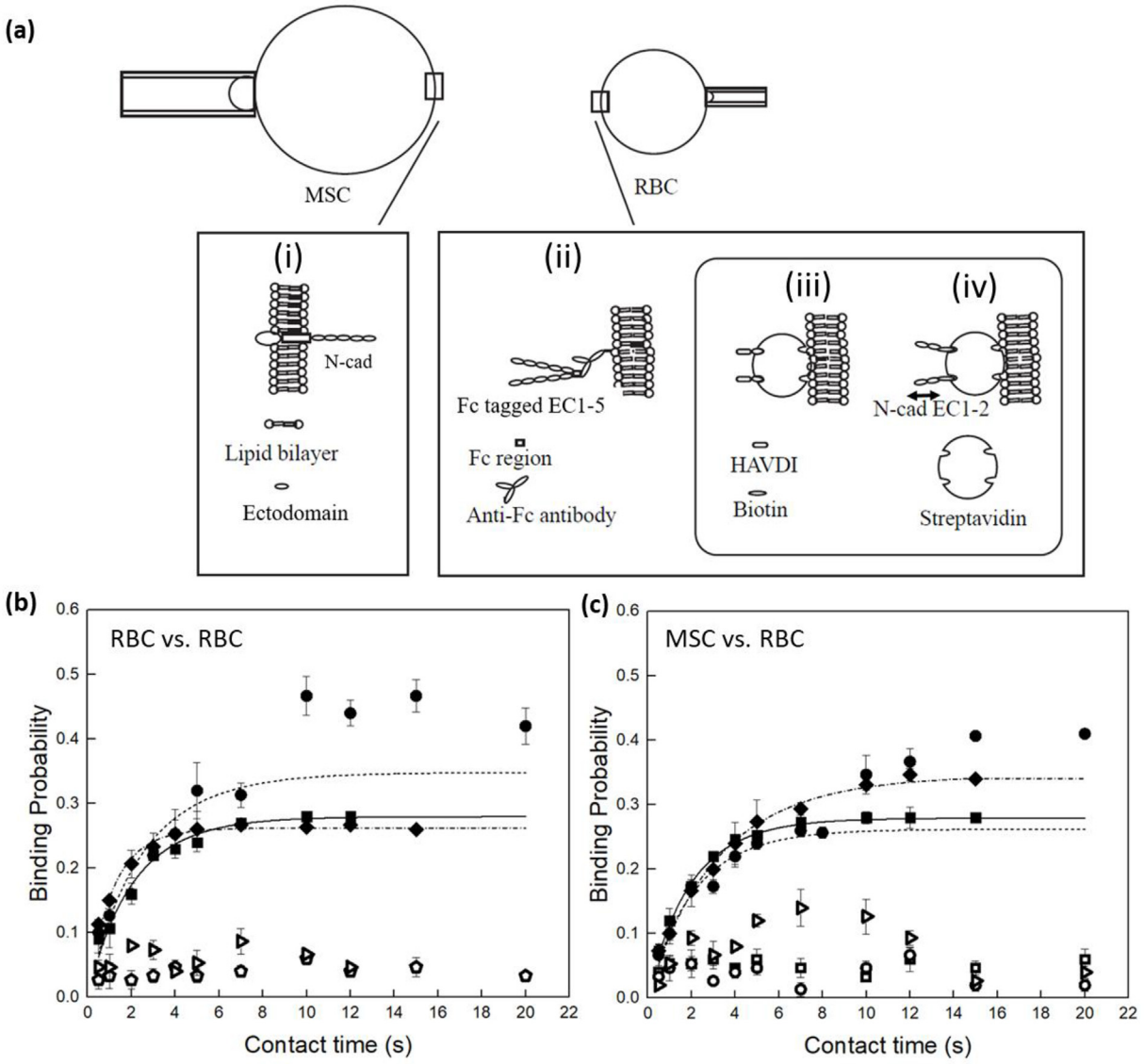

Fig. 8. Binding probability versus contact time between N-cadherin ligands on opposing RBCs or between N-cadherin ligands on an RBC and N-cadherin on MSCs. (a) Schematic of the micropipette frequency assay setup. (a–i) MSC expressing membrane bound wild type N-cadherin is aspirated using a micropipette of diameter ~ 7 μm^2. The other micropipette has a diameter ~1.5 μm^2 and is used to aspirate a red blood cell (RBC) modified with N-cadherin ligands. For affinity measurement experiments, (a-ii) Fc-tagged N-cad EC1-5 is covalently attached with anti-Fc antibody on the RBC membrane and both (a-ii) biotinylated HAVDI peptide and (a-iv) biotinylated N-cad EC1-2 are attached to streptavidin coated RBC membrane. (b) Binding probability versus contact time between RBCs displaying different N-cadherin fragments. Data shown include measurements between N-cad EC1-5 fragments on opposing RBCs (black circles); between N-cad EC1-5 and N-cad EC1-2 (black diamonds); and between N-cad EC1-5 and HAVDI (black squares). Controls shown include measurements between RBCs without N-cad fragments (white trapezoids) and between scrambled peptide and N-cad EC 1–5 immobilized on RBC (white triangles). The data shown are the average ± s. e.m. The cadherin densities on the two cells are given in Table 1. The dashed and solid lines through the data are the nonlinear least squares fits of the data (EC1 binding step) to Eq. (4), with best-fit parameters given in the text and in Table 1. (c) Binding probability versus contact time between RBCs displaying different N-cadherin fragments and MSCs. Data shown include measurements with RBCs displaying N-cad EC1-5 fragments (black circles); N-cad EC1-2 (black diamonds); and HAVDI (black squares). Controls shown include measurements between MSCs and RBCs modified with anti-Fc antibody (white circles) or streptavidin (white squares) or scrambled peptides (white triangles). The data shown are the average ± s. e.m. The dashed and solid lines through the data are the nonlinear least squares fits of the data for EC1 binding to Eq. (4), with best fit parameters given in the text and in Table 1.

consistent correlation between the cell behaviors examined and the measured affinities of the different fragments for cell surface N-cadherin. The present results do not establish the mechanism(s) underlying the biochemical differences. However, the results reveal that truncating the extracellular region of N-cadherin alters cell signaling, and these differences should be considered when selecting the fragment used for fundamental studies or for therapeutic applications. As a result, the choice of the N-cadherin fragment would be particularly relevant for the design of biomaterials to regulate cell functions.

Data availability statement

The raw/processed data required to reproduce these findings cannot be shared at this time as the data also forms part of an ongoing study.

Acknowledgements

This work was supported by the National Science Foundation ([CBET-1403491 & 1932192] to H.K. & D.E.L., Graduate Research Fellowship Program [DGE – 1144245] to E.C.Q, and the Integrative

Table 1
Best fit parameters from nonlinear least squares fits of binding between N-cadherin ligands (N-cad EC1-5, N-cad EC1-2, or HAVDI) on RBCs and either wild type N-cadherin on MSCs or N-cad EC1-5 on RBCs. Cell 1 and cell 2 refer to the two opposing cells in the adhesion frequency measurements, as illustrated in Fig. 8a.

Cell 1	Ligand 1	Ligand 1 Density (number/μm^2)	Cell 2	Ligand 2	Ligand 2 Density (number/μm^2)	Affinity (10^{-5} μm^2)
RBC	N-cad EC1-5	20	RBC	N-cad EC1-5	20	14.8 ± 0.4
		14		N-cad EC1-2	40	7.5 ± 0.1
		32		HAVDI	18	7.9 ± 0.1
MSC	N-cad WT	11	RBC	N-cad EC1-5	28	14.0 ± 0.1
		26		N-cad EC1-2	40	7.3 ± 0.2
		11		HAVDI	52	7.95 ± 0.02

Graduate Education and Research Traineeship: Training the Next Generation of Researchers in Cellular and Molecular Mechanics and Bionanotechnology [Grant 0965918] to E.C.Q). The authors would like to thank Prof. Huimin Zhao and Dr. Bin Wang for the use of and help with the High-Performance Liquid Chromatography. Experiments were carried out in part at the Carl R. Woese Institute for Genomic Biology at the University of Illinois.

Appendix A. Supplementary data

Supplementary data to this article can be found online at https://doi.org/10.1016/j.biomaterials.2020.119846.

References

[1] J.M. Halbleib, W.J. Nelson, Cadherins in development: cell adhesion, sorting, and tissue morphogenesis, Genes Dev. 20 (2006) 3199–3214.
[2] M. Takeichi, Morphogenetic roles of classic cadherins, Curr. Opin. Cell Biol. 7 (1995) 619–627.
[3] M. Takeichi, Cadherins: a molecular family important in selective cell-cell adhesion, Annu. Rev. Biochem. 59 (1990) 237–252.
[4] B.M. Gumbiner, Regulation of cadherin-mediated adhesion in morphogenesis, Nat. Rev. Mol. Cell Biol. 6 (2005) 622–634.
[5] B.M. Gumbiner, Cell adhesion: the molecular basis of tissue architecture and morphogenesis, Cell 84 (1996) 345–357.
[6] C.M. Niessen, D. Leckband, A.S. Yap, Tissue organization by cadherin adhesion molecules: dynamic molecular and cellular mechanisms of morphogenetic regulation, Physiol. Rev. 91 (2011) 691–731.
[7] A. Nose, A. Nagafuchi, M. Takeichi, Expressed recombinant cadherins mediate cell sorting in model systems, Cell 54 (1988) 993–1001.
[8] M.S. Steinberg, M. Takeichi, Experimental specification of cell sorting, tissue spreading, and specific spatial patterning by quantitative differences in cadherin expression, Proc. Natl. Acad. Sci. U.S.A. 91 (1994) 206–209.
[9] R.B. Hazan, G.R. Phillips, R.F. Qiao, L. Norton, S.A. Aaronson, Exogenous expression of N-cadherin in breast cancer cells induces cell migration, invasion, and metastasis, J. Cell Biol. 148 (2000) 779–790.
[10] O. Thoumine, M. Lambert, R.M. Mege, D. Choquet, Regulation of N-cadherin dynamics at neuronal contacts by ligand binding and cytoskeletal coupling, Mol. Biol. Cell 17 (2005) 862–875.
[11] N.K. Noren, C.M. Niessen, B.M. Gumbiner, K. Burridge, Cadherin engagement regulates rho family GTPases, J. Biol. Chem. 276 (2001) 33305–33308.
[12] L.D.M. Derycke, M.E. Bracke, N-cadherin in the spotlight of cell-cell adhesion, differentiation, invasion and signalling, Int. J. Dev. Biol. 48 (2004) 463–476.
[13] S.-L. Cheng, F. Lecanda, M.K. Davidson, P.M. Warlow, S.-F. Zhang, L. Zhang, S. Suzuki, T. St John, R. Civitelli, Human osteoblasts express a repertoire of cadherins, which are critical for BMP-2-induced osteogenic differentiation, J. Bone Miner. Res. 13 (1998) 633–644.
[14] M. George-Weinstein, J. Gerhart, J. Blitz, E. Simak, K.A. Knudsen, N-cadherin promotes the commitment and differentiation of skeletal muscle precursor cells, Dev. Biol. 185 (1997) 14–24.
[15] A. Stockinger, A. Eger, J. Wolf, H. Beug, R. Foisner, E-cadherin regulates cell growth by modulating proliferation-dependent β-catenin transcriptional activity, J. Cell Biol. 154 (2001) 1185–1196.
[16] N.-G. Kim, E. Koh, X. Chen, B.M. Gumbiner, E-cadherin mediates contact inhibition of proliferation through hippo signaling-pathway components, Proc. Natl. Acad. Sci. Unit. States Am. 108 (2011) 11930–11935.
[17] M.G. Lampugnani, A. Zanetti, M. Corada, T. Takahashi, G. Balconi, F. Breviario, F. Orsenigo, A. Cattelino, R. Kemler, T.O. Daniel, E. Dejana, Contact inhibition of VEGF-induced proliferation requires vascular endothelial cadherin, β-catenin, and the phosphatase DEP-1/cd148, J. Cell Biol. 161 (2003) 793–804.
[18] D.E. Leckband, J. de Rooij, Cadherin adhesion and mechanotransduction, Annu. Rev. Cell Dev. Biol. 30 (2014) 291–315.
[19] E. Ruoslahti, RGD and other recognition sequences for integrins, Annu. Rev. Cell Dev. Biol. 12 (1996) 697–715.
[20] L. Shapiro, W.I. Weis, Structure and biochemistry of cadherins and catenins, Cold Spring Harb. Perspect. Biol. 1 (2009) a003053.
[21] B.D. Cosgrove, K.L. Mui, T.P. Driscoll, S.R. Caliari, K.D. Mehta, R.K. Assoian, J.A. Burdick, R.L. Mauck, N-cadherin adhesive interactions modulate matrix mechanosensing and fate commitment of mesenchymal stem cells, Nat. Mater. 15 (2016) 1297–1306.
[22] T.H. Qazi, D.J. Mooney, G.N. Duda, S. Geissler, Biomaterials that promote cell-cell interactions enhance the paracrine function of MSCs, Biomaterials 140 (2017) 103–114.
[23] E. Ju Lee, E.-K. Choi, S. Kyoung Kang, G.-H. Kim, J. Young Park, H.-J. Kang, S.-W. Lee, K.-H. Kim, J. Sook Kwon, K. Hong Lee, Y. Ahn, H.-J. Lee, H.-J. Cho, S. Jin Choi, W. Il Oh, Y.-B. Park, H.-S. Kim, N-cadherin determines individual variations in the therapeutic efficacy of human umbilical cord blood-derived mesenchymal stem cells in a rat model of myocardial infarction, Mol. Ther. 20 (2012) 155–167.
[24] T.H. Qazi, D.J. Mooney, G.N. Duda, S. Geissler, Niche-mimicking interactions in peptide-functionalized 3D hydrogels amplify mesenchymal stromal cell paracrine effects, Biomaterials 230 (2020) 119639.
[25] L. Bian, M. Guvendiren, R.L. Mauck, J.A. Burdick, Hydrogels that mimic developmentally relevant matrix and N-cadherin interactions enhance MSC chondrogenesis, Proc. Natl. Acad. Sci. U.S.A. 110 (2013) 10117–10122.
[26] M.Y. Kwon, S.L. Vega, W.M. Gramlich, M. Kim, R.L. Mauck, J.A. Burdick, Dose and timing of N-cadherin mimetic peptides regulate MSC chondrogenesis within hydrogels, Adv. Healthc. Mater. 7 (2018) 1701199.
[27] X.S. Yue, Y. Murakami, T. Tamai, M. Nagaoka, C.S. Cho, Y. Ito, T. Akaike, A fusion protein N-Cadherin-Fc as an artificial extracellular matrix surface for maintenance of stem cell features, Biomaterials 31 (2010) 5287–5296.
[28] J.C.M. Vega L, M.K. Lee, E.C. Qin, M. Rich, K.Y. Lee, D.H. Kim, H.J. Chung, D.E. Leckband, H. Kong, Three dimensional conjugation of recombinant N-cadherin to a hydrogel for in vitro anisotropic neural growth, J. Mater. Chem. B. 4 (2016) 6803–6811.
[29] J.L. Bixby, R. Zhang, Purified N-cadherin is a potent substrate for the rapid induction of neurite outgrowth, J. Cell Biol. 110 (1990) 1253–1260.
[30] E.C. Qin, M.E. Kandel, E. Liamas, T.B. Shah, C. Kim, C.D. Kaufman, Z.J. Zhang, G. Popescu, M.U. Gillette, D.E. Leckband, H. Kong, Graphene oxide substrates with N-cadherin stimulates neuronal growth and intracellular transport, Acta Biomater. 90 (2019) 412–423.
[31] M. Lambert, F. Padilla, R.M. Mège, Immobilized dimers of N-cadherin-Fc chimera mimic cadherin-mediated cell contact formation: contribution of both outside-in and inside-out signals, J. Cell Sci. 113 (2000) 2207–2219.
[32] A. Ganz, M. Lambert, A. Saez, P. Silberzan, A. Buguin, R.M. Mège, B. Ladoux, Traction forces exerted through N-cadherin contacts, Biol. Cell. 98 (2006) 721–730.
[33] J. Gavard, V. Marthiens, C. Monnet, M. Lambert, R.M. Mège, N-cadherin activation substitutes for the cell contact control in cell cycle arrest and myogenic differentiation: involvement of p120 and β-catenin, J. Biol. Chem. 279 (2004) 36795–36802.
[34] M. Zhu, S. Lin, Y. Sun, Q. Feng, G. Li, L. Bian, Hydrogels functionalized with N-cadherin mimetic peptide enhance osteogenesis of hMSCs by emulating the osteogenic niche, Biomaterials 77 (2016) 44–52.
[35] R. Li, J. Xu, D.S.H. Wong, J. Li, P. Zhao, L. Bian, Self-assembled N-cadherin mimetic peptide hydrogels promote the chondrogenesis of mesenchymal stem cells through inhibition of canonical Wnt/β-catenin signaling, Biomaterials 145 (2017) 33–43.
[36] T.J. Boggon, J. Murray, S. Chappuis-Flament, E. Wong, B.M. Gumbiner, L. Shapiro, C-cadherin ectodomain structure and implications for cell adhesion mechanisms, Science 296 (80) (2002) 1308–1313.
[37] K. Tamura, W.S. Shan, W.A. Hendrickson, D.R. Colman, L. Shapiro, Structure-function analysis of cell adhesion by neural (N-) cadherin, Neuron 20 (1998) 1153–1163.
[38] L. Shapiro, a M. Fannon, P.D. Kwong, A. Thompson, M.S. Lehmann, G. Grübel, J.F. Legrand, J. Als-Nielsen, D.R. Colman, W.A. Hendrickson, Structural basis of cell-cell adhesion by cadherins, Nature 374 (1995) 327–337.
[39] O.W. Blaschuk, R. Sullivan, S. David, Y. Pouliot, Identification of a cadherin cell adhesion recognition sequence, Dev. Biol. 139 (1990) 227–229.
[40] K. Tamura, W.-S.S. Shan, W.A. Hendrickson, D.R. Colman, L. Shapiro, Structure-function analysis of cell adhesion by neural (N-) cadherin, Neuron 20 (1998) 1153–1163.
[41] S.D. Skaper, L. Facci, G. Williams, E.J. Williams, F.S. Walsh, P. Doherty, A dimeric version of the short N-cadherin binding motif HAVDI promotes neuronal cell survival by activating an N-cadherin/fibroblast growth factor receptor signalling cascade, Mol. Cell. Neurosci. 26 (2004) 17–23.
[42] P. Doherty, E. Williams, O.W. Blaschuk, G. Williams, B.J. Gour, A novel family of cyclic peptide antagonists suggests that N-cadherin specificity is determined by amino acids that flank the HAV motif, J. Biol. Chem. 275 (2002) 4007–4012.
[43] S. Rakshit, Y. Zhang, K. Manibog, O. Shafraz, S. Sivasankar, Ideal, catch, and slip

bonds in cadherin adhesion, Proc. Natl. Acad. Sci. Unit. States Am. 109 (2012) 18815–18820.
[44] K. Manibog, H. Li, S. Rakshit, S. Sivasankar, Resolving the molecular mechanism of cadherin catch bond formation, Nat. Commun. 5 (2014) 3941.
[45] O.J. Harrison, F. Bahna, P.S. Katsamba, X. Jin, J. Brasch, J. Vendome, G. Ahlsen, K.J. Carroll, S.R. Price, B. Honig, L. Shapiro, Two-step adhesive binding by classical cadherins, Nat. Struct. Mol. Biol. 17 (2010) 348–357.
[46] A.K. Prakasam, V. Maruthamuthu, D.E. Leckband, Similarities between heterophilic and homophilic cadherin adhesion, Proc. Natl. Acad. Sci. Unit. States Am. 103 (2006) 15434–15439.
[47] S. Sivasankar, B. Gumbiner, D. Leckband, Direct measurements of multiple adhesive alignments and unbinding trajectories between cadherin extracellular domains, Biophys. J. 80 (2001) 1758–1768.
[48] S. Chappuis-Flament, E. Wong, L.D. Hicks, C.M. Kay, B.M. Gumbiner, Multiple cadherin extracellular repeats mediate homophilic binding and adhesion, J. Cell Biol. 154 (2001) 231–243.
[49] Y.H. Chien, N. Jiang, F. Li, F. Zhang, C. Zhu, D. Leckband, Two stage cadherin kinetics require multiple extracellular domains but not the cytoplasmic region, J. Biol. Chem. 283 (2008) 1848–1856.
[50] Y. Wu, P. Kanchanawong, R. Zaidel-Bar, Actin-delimited adhesion-independent clustering of E-cadherin forms the nanoscale building blocks of adherens junctions, Dev. Cell 32 (2015) 139–154.
[51] N. Shashikanth, M.A. Kisting, D.E. Leckband, Kinetic measurements reveal enhanced protein-protein interactions at intercellular junctions, Sci. Rep. 6 (2016) 23623.
[52] M.D. Langer, H. Guo, N. Shashikanth, J.M. Pierce, D.E. Leckband, N-glycosylation alters cadherin-mediated intercellular binding kinetics, J. Cell Sci. 125 (2012) 2478–2485.
[53] T.W. Morris, J.E. Cronan, D.L. Turner, J.C. Wallace, A. Chapman-Smith, Expression, biotinylation and purification of a biotin-domain peptide from the biotin carboxy carrier protein of Escherichia coli acetyl-CoA carboxylase, Biochem. J. 302 (2015) 881–887.
[54] J.R. Tse, A.J. Engler, Preparation of hydrogel substrates with tunable mechanical properties, Curr. Protoc. Cell Biol. (2010) 1–16.
[55] S. Sen, A.J. Engler, D.E. Discher, Matrix strains induced by cells: computing how far cells can feel, Cell. Mol. Bioeng. 2 (2009) 39–48.
[56] J.P. Butler, I.M. Tolic-Norrelykke, B. Fabry, J.J. Fredberg, Traction fields, moments, and strain energy that cells exert on their surroundings, AJP Cell Physiol 282 (2002) C595–C605.
[57] K.A. Beningo, C.M. Lo, Y.L. Wang, Flexible polyacrylamide substrata for the analysis of mechanical interactions at cell-substratum adhesions, Methods Cell Biol. (2002) (2002) 325–339.
[58] E.R. Gold, H.H. Fudenberg, Chromic chloride: a coupling reagent for passive hemagglutination reactions, J. Immunol. 99 (1967) 859–866.
[59] R. Kofler, G. Wick, Some methodologic aspects of the chromium chloride method for coupling antigen to erythrocytes, J. Immunol. Methods 16 (1977) 201–209.
[60] S.E. Chesla, P. Selvaraj, C. Zhu, Measuring two-dimensional receptor-ligand binding kinetics by micropipette, Biophys. J. 75 (1998) 1553–1572.
[61] C. Cozens-Roberts, D.A. Lauffenburger, J.A. Quinn, Receptor-mediated cell attachment and detachment kinetics, Biophys. J. 58 (1990) 841–856.
[62] J.W. Neill, Testing for lack of fit in nonlinear regression, Ann. Stat. 16 (1988) 733–740.
[63] K.J. Lee, Q. Shi, A.K. Barry, H. Tabdili, Y.-H. Chien, S. Lu, M.D. Langer, D.E. Leckband, Cadherin point mutations alter cell sorting and modulate GTPase signaling, J. Cell Sci. 125 (2012) 3299–3309.
[64] A.J. Engler, M.A. Griffin, S. Sen, C.G. Bönnemann, H.L. Sweeney, D.E. Discher, Myotubes differentiate optimally on substrates with tissue-like stiffness: pathological implications for soft or stiff microenvironments, J. Cell Biol. 166 (2004) 877–887.
[65] A.J. Engler, S. Sen, H.L. Sweeney, D.E. Discher, Matrix elasticity directs stem cell lineage specification, Cell 126 (2006) 677–689.
[66] H. Tabdili, M. Langer, Q. Shi, Y.-C. Poh, N. Wang, D. Leckband, Cadherin-dependent mechanotransduction depends on ligand identity but not affinity, J. Cell Sci. 125 (2012) 4362–4371.
[67] B.A. Bryan, T.E. Walshe, D.C. Mitchell, J.S. Havumaki, M. Saint-Geniez, A.S. Maharaj, A.E. Maldonado, P.A. D'amore, Coordinated vascular endothelial growth factor expression and signaling during skeletal myogenic differentiation, Mol. Biol. Cell 19 (2008) 994–1006.
[68] N. Arsic, S. Zacchigna, L. Zentilin, G. Ramirez-Correa, L. Pattarini, A. Salvi, G. Sinagra, M. Giacca, Vascular endothelial growth factor stimulates skeletal muscle regeneration in Vivo, Mol. Ther. 10 (2004) 844–854.
[69] H.H. Vandenburgh, P. Karlisch, J. Shansky, R. Feldstein, Insulin and IGF-I induce pronounced hypertrophy of skeletal myofibers in tissue culture, Am. J. Physiol. 260 (1991) C475–C484.
[70] C. Duan, H. Ren, S. Gao, Insulin-like growth factors (IGFs), IGF receptors, and IGF-binding proteins: roles in skeletal muscle growth and differentiation, Gen. Comp. Endocrinol. 167 (2010) 344–351.
[71] J.S. Chamberlain, J.B. Jaynes, S.D. Hauschka, Regulation of creatine kinase induction in differentiating mouse myoblasts, Mol. Cell Biol. 5 (1985) 484–492.
[72] J.B. Jaynes, J.S. Chamberlain, J.N. Buskin, J.E. Johnson, S.D. Hauschka, Transcriptional regulation of the muscle creatine kinase gene and regulated expression in transfected mouse myoblasts, Mol. Cell Biol. 6 (1986) 2855–2864.
[73] N. Shashikanth, Y.I. Petrova, S. Park, J. Chekan, S. Maiden, M. Spano, T. Ha, B.M. Gumbiner, D.E. Leckband, Allosteric regulation of E-cadherin adhesion, J. Biol. Chem. 290 (2015) 21749–21761.
[74] P. Katsamba, K. Carroll, G. Ahlsen, F. Bahna, J. Vendome, S. Posy, M. Rajebhosale, S. Price, T.M. Jessell, A. Ben-Shaul, L. Shapiro, B.H. Honig, Linking molecular affinity and cellular specificity in cadherin-mediated adhesion, Proc. Natl. Acad. Sci. Unit. States Am. 106 (2009) 1594–11599.
[75] A. Prakasam, Y.H. Chien, V. Maruthamuthu, D.E. Leckband, Calcium site mutations in cadherin: impact on adhesion and evidence of cooperativity, Biochemistry 45 (2006) 6930–6939.
[76] G. Handschuh, B. Luber, P. Hutzler, H. Höfler, K.F. Becker, Single amino acid substitutions in conserved extracellular domains of E-cadherin differ in their functional consequences, J. Mol. Biol. 314 (2001) 445–454.
[77] T. Nguyen, L. Duchesne, G.H.N. Sankara Narayana, N. Boggetto, D.D. Fernig, C. Uttamrao Murade, B. Ladoux, R.M. Mège, Enhanced cell–cell contact stability and decreased N-cadherin-mediated migration upon fibroblast growth factor receptor-N-cadherin cross talk, Oncogene 38 (2019) 6283–6300.
[78] P. Doherty, F.S. Walsh, CAM-FGF receptor interactions: a model for axonal growth, Mol. Cell. Neurosci. 8 (1996) 99–111.